공학박사학위논문

# Fabrication of 2-D Protein Films and 3-D Protein Microspheres Based on Alternative Self-Assembly of α-Synuclein and their Applications

알파-시누클레인의 대체자가결합을 이용한 2차원 단백질 필름과 3차원 단백질 마이크로스피어의 제작과 응용

2020년 2월

서울대학교 대학원

화학생물공학부

이 순 구

# Abstract

## Fabrication of 2-D Protein Films and 3-D Protein Microspheres Based on Alternative Self-Assembly of α-Synuclein and their Applications

Soonkoo Lee

School of Chemical and Biological Engineering

The Graduate School

Seoul National University

Understanding polymorphism of self-assembly process and alternative self-assembly of amyloidogenic proteins is valuable not only to find their pathological implications but also to prepare protein-based biomaterials. α-Synuclein is one of the amyloidogenic protein closely related to degenerative

disease, Parkinson's disease. α-Synuclein (αS), producing one-dimensional (1-D) amyloid fibrils, has been employed to generate two-dimensional (2-D) protein films and three-dimensional (3-D) protein microspheres via its alternative self-assembly at either high temperature or rapid-freezing condition`, respectively. At a high temperature of 50 °C, αS molecules self-assembled into the 2-D film whereas 1-D amyloid fibrils were produced at 37 °C. This alternative self-assembly phenomenon could be attributed to structural plasticity of the intrinsically disordered protein of αS which turns into a surface active agent at the air-water interface at the high temperature. The αS 2-D film was also routinely prepared at the oil-water interface with larger scale and the film was excellent in cell adhesion and adsorbed well with αS-coated nanoparticles, suggesting its potential as a biomaterial. αS film was also used as a framework of molecular assembly to give rise to a polydiacetylene-based sensing material. 10,12-Pentacosadiynoic acids (PCDA) were aligned on the film in a spatially organized way and then photo-polymerized to induce the π-conjugated molecular assembly yielding blue color. Its colorimetric transition to red was induced by increasing temperature, pH, and organic solvents. This functionalize d protein film increased its height to 55 nm from 40 nm upon the PCDA immobilization and exhibited enhanced physical and chemical stability. In addition, the modified film showed remarkable high electrical conductivity only in the red state. Under frozen condition, on the other hand, protein microspheres were produced from αS

oligomers via rapid freezing, frozen annealing, and freeze-drying process. αS microspheres prepared with αS-eosin conjugates and focused ion-beam severance of αS microspheres confirmed their empty core structure. αS microspheres showed remarkable stability at room temperature without chemical additives or cross linkers. While microspheres were stable at room temperature, they were immediately converted into amyloid burs comprised of nano fibrils upon heating. Therefore, protein microspheres could be considered a constrained spherical structure transformable into biocompatible matrix material in nanoscale which could be used as a fill-in agent to improve mechanical strength of living tissues like skin as well as hydrogels in general. In this study, selective fabrication of the potential protein-based biomaterials have been demonstrated.

**Keywords**

**α-Synuclein, Intrinsically Disordered Protein, Alternative Self-assembly, Polydiacetylene, Protein Film, Protein Microsphere, Amyloid Bur**

**Student Number**

**2009-21013**

# Contents

## List of Figures

# Part I.

# Fabrication of α-Synuclein Film and its Applications

## I-1. Introduction

### (1) Amyloidogenesis

Amyloidogenesis of proteins is closely related to various diseases, from neurodegenerative diseases such as Parkinson's disease (PD)[1-3], Alzheimer's disease (AD)[4-5], Huntington's disease[6] to non-neuropathic diseases such as Type II diabetes[7], even non-neuropathic diseases such as cartaract.[8] Amyloidogenic proteins form insoluble protein nanofibrils scales between 5 nm ~ 15 nm width and multi-micro scale length through amyloidogenesis.[9] Despite its close association with various diseases, the mechanism of amyloid formation process has not yet been clearly defined.[10] Amyloid fibers formed by amyloidogenic proteins are called amyloid fibrils (AFs), stabilized via a regular

internal structure of cross β-sheet conformation[8], material value of amyloid fibrils has been appreciated on the basis of their exceptional properties such as physical and chemical stability,[11] mechanical strength,[12] self-propagating structural polymorphism and thus used for fibrillar amplification,[13] template for chemical modifications,[14] hydrogel formation with nano-scaled mesh for an effective enzyme entrapment,[15] and a considerable cell surface interaction.[16]

## (2) α-Synuclein (αS) : Intrinsically disordered protein

α-Synuclein (αS) is amyloidogenic protein known to be closely related to Parkinson's disease (PD)[1-3]. αS is intrinsically disordered protein (IDP) exhibits random structure, which means specific structure of protein is not defined in their monomer state,[17-18] showing multiple ligand interaction with physiological or non-physiological partners.[19] Based on this structural plasticity, αS can be converted into various structures. In case of binding with negative charged lipid membrane, αS forms α-helical structure[20-21], while in case of binding with neutral lipid, αS shows β-sheet structure forming radiating amyloid fibrils (RAFs)[22]. The structural plasticity of αS is the theoretical background that the result of αS self-assembly may not be the only amyloid fiber.

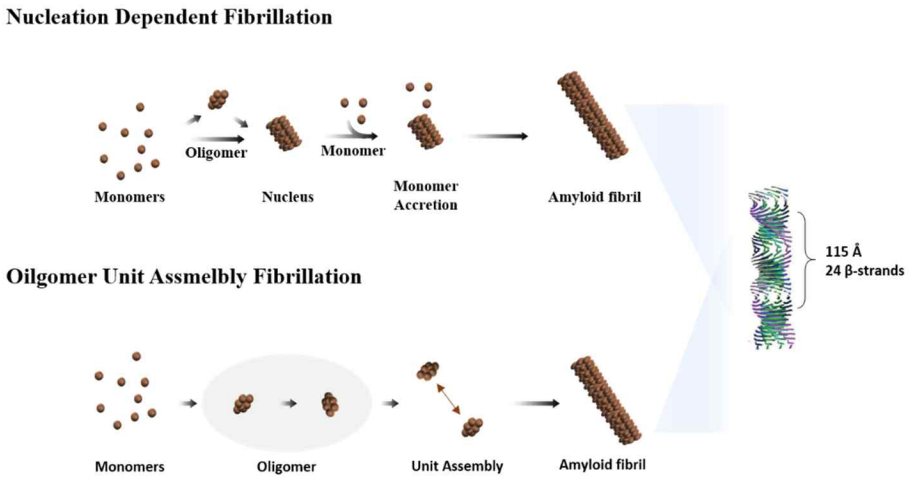


**Figure 1. Mechanisms of α-synuclein (αS) fibrillation.** Nucleation dependent fibrillation and oligomer unit assembly fibrillation models as representative mechanism models on αS self-assembly of fibril formation.

## (3) Mechanism of αS fibrillation

In general, fibrillation process of αS to form amyloid fibrils can be explained by two theories (Figure 1), although no specific mechanism has been proved, the phenomenological changes in structure and the characteristics of each structure. The first model is nucleation dependent fibrillation. In this model, αS monomers form oligomers through self-assembly, and one oligomer promotes fibrosis by acting as a nucleus for restructuring fibrillated αS monomers which are not yet oligomers. Nucleation-dependent fibrillation as a widely recognized mechanism requires the preformed nuclei which readily grow into the fibrils through selective accretion of amyloidogenic proteins with a considerable structural adjustment[8, 23]. Alternatively, self-association based on unit assembly of oligomers has also been proposed.[24] The self-assembly produces the same oligomers from the αS monomer, but each oligomer acts as a blocking block to form amyloid fibrils. The amyloid structure formed through self-assembly shows a lattice-shaped β-sheet structure, which shows high strength due to hydrogen bonding between protein skeletons. The formed amyloid has high stability in aqueous solution and has a very regular structure, so it has high strength and excellent applicability as a bio-material.

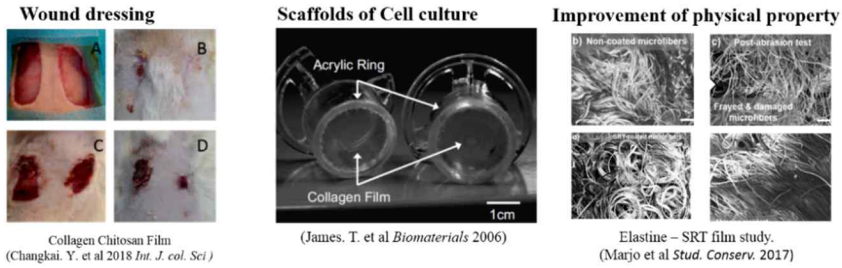


**Figure 2. Applications of protein films.** Protein film has been applied to various fields based on biocompatible properties. Collagen and chitosan films prevent wounds from contaminations (Changkai. Y. et al 2018 *Int. J. col. Sci)*, collagen film suggests a basic framework for cell growth (James. T. et al *Biomaterials* 2006), and coat other materials to obtain physical properties (Marjo et al *Stud. Conserv.* 2017).

## (4) Protein films

Protein films can be used in various areas from biomedical engineering to environmental science (Figure 2).[25-30] They can be grafted to conventional materials such as metals, ceramics, and polymers not only to alter their innate physical and chemical properties, but also to convert the surfaces to be biocompatible,[31-34] which could be further functionalized by immobilizing biologically or chemically active agents to elicit diverse activities useful for as a scaffold where cells grow, anti-microbial film, wound dressing, tissue engineering including scaffold of cell culture, controlled drug release, and sensor development.[35-41] For the sensor development in particular, the protein films require decent stability overcoming their inherent fragility in addition to sensitivity to external stimuli which need to be transformed into detectable responses.

# I-2. Results and discussion

## (1) Film formation of αS

αS showed alternative molecular self-assembly leading to either amyloid

fibril or protein film formation. αS self-assembled to amyloid fibrils in bulk solution at 37 ºC after a prolonged incubation for 14 days whereas protein films were produced at air-water interface when incubated at 50 ºC for 3 days under a quiescent condition (Figure 3). The films started to appear from 2 days of incubation while the 37 ºC incubated fibrils were far yet to be produced (Figure 3A and 3B).

## (2) Structural analysis of αS film

Circular dichroism spectrometer (CD) and fourier transformation infrared spectrophotometer (FTIR) with attenuated total reflectance (ATR) mode were measured to determine the structural characteristics of αS film. The CD analyses showed a small increase in the minimum ellipticity at 198 nm compared with αS monomers. This fact indicated that the films were assembled with αS still existing in a disordered state because monomeric state of αS is well known to exist as random structure. On the other hand, amyloid fibril from the same monomeric spices of αS was observed with a drastic conformational change from the random to β-sheet structure as determined by the shift in the wavelength of the minimum ellipticity from 198 nm to 219 nm (Figure 4). In the FTIR spectra, the dashed line indicates the monomer spectra. The FTIR of film structure analyses indicated that the films were produced by transforming

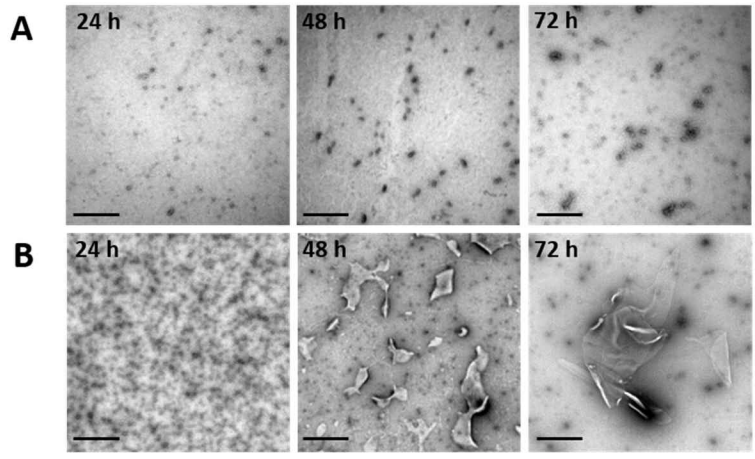


**Figure 3. Formation of αS film structure.** Film formation of αS was observed by electron microscopy. αS formed a short fibrous structure at 37 °C quiescent incubation (A), but formed a film structure at 50 °C (B) quiescent incubation of 24 h, 48 h and 72 h respectively.

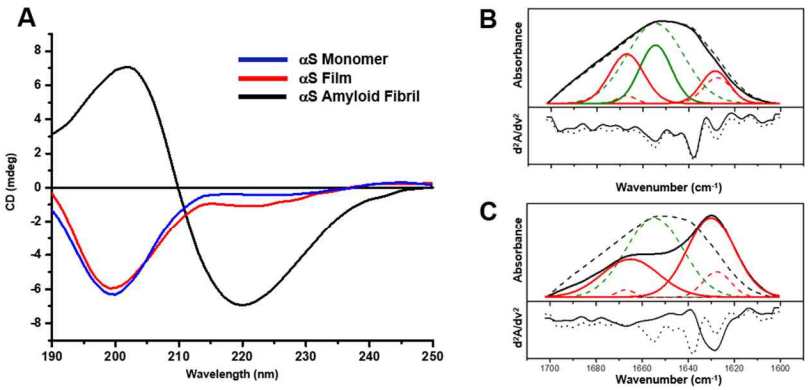


**Figure 4. Structural analysis of αS Film.** In order to analyze the secondary structure of the protein constituting the αS film, the structure was analyzed in comparison with αS monomers and αS amyloid fibrils. (A) CD analysis (B) FTIR data of αS film structure (solid line: film, dotted line: monomers) comparison with (C) FTIR data of fibril structure (solid line: fibril, dotted line: monomers)

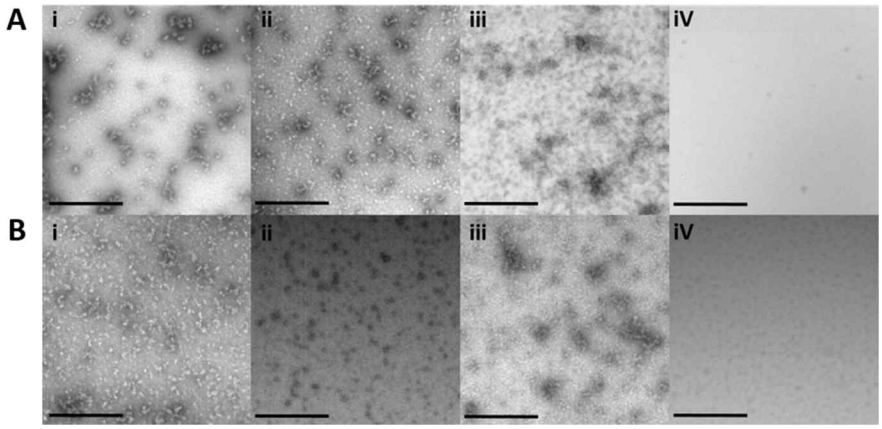


**Figure 5. TEM images of various proteins after 48 h of quiescent incubations.** TEM images of proteins at either 37 ℃ (A) or 50 ℃ (B). The proteins include α-lactalbumin (i), β-lactoglobulin (ii), bovine serum albumin (iii), and elastin (iv). Scale bars represent 500 nm.

some of the random structure (1653 $cm^{-1}$) into mostly the turn structure at ca. 1667 $cm^{-1}$ with a slight increase in the β-sheet structure at ca. 1628 $cm^{-1}$ as found in the decomposed spectrum of the deconvolved spectrum (amide I band) with 2nd derivative monitored for the films in comparison with that of monomeric αS (Figure 4B).[42] In contrast, the amyloid fibrils were generated with a simultaneous increase in the two components at ca. 1628 and 1667 $cm^{-1}$ designated for the β-sheets and turns. And the component (1653 $cm^{-1}$) for the random structure was completely diminished (Figure 4C). Taken together, it could be suggested that the films have been generated by forming another non-regular structure of the turns which are certainly distinctive from the random structure found in the monomeric αS although their structural details need to be clarified.

## (3) αS specific film formation

Film formation was unique to αS since other proteins such as α-lactalbumin, β-lactoglobulin, bovine serum albumin, and elastin were not able to produce the film when incubated at 50 ºC for 2 days (Figure 5). In order to confirm whether the film-forming phenomenon is specific to αS, an experiment using αS Y136C mutant was conducted. The production of fluorescent 2D film with

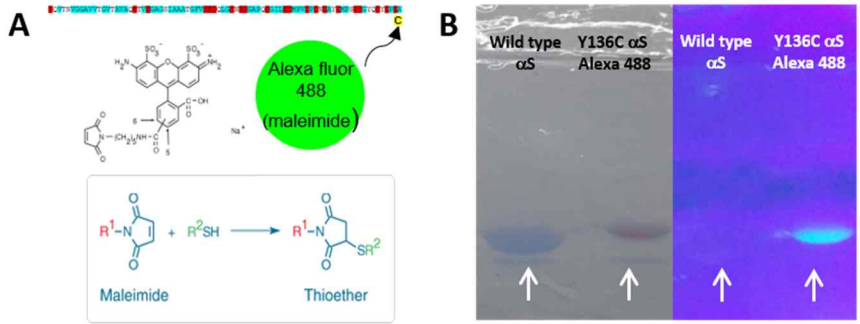


**Figure 6. Preparation of αS Y136C mutant conjugated with Alexa Fluor 488.** (A) Schematic representation mutant αS of Y136C conjugated with Alexa Flour 488. (B) Labeling of the fluorescent dye, Alexa Fluor 488 to αS was confirmed with SDS-PAGE with UV irradiation. The unreacted residual dye was removed with the C4-reversed phase HPLC.

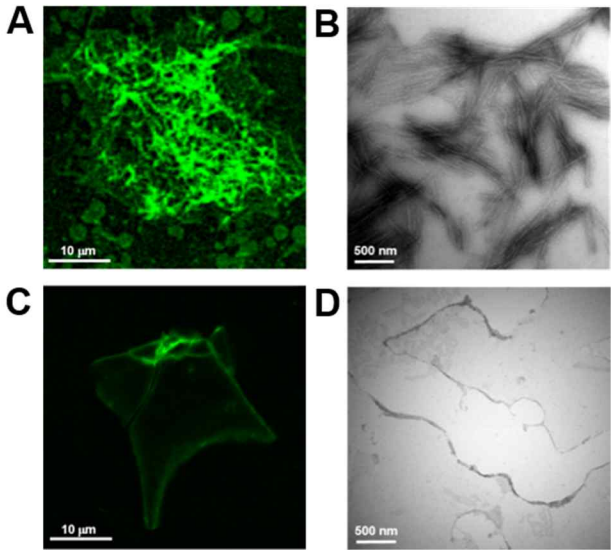


**Figure 7. Film formation of αS-Alexa 488.** αS film formation was confirmed through incubation of the Alexa 488 tagged αS Y136C mutant. At 37 ℃ shaking incubation of αS, fibril formation of observed with confocal microscope (A), and TEM (B). At 50 ℃ quiescent incubation of αS, film formation of observed with confocal microscope (C), and TEM (D).

the αS labeled with Alexa-488 (αS-Alexa-488) at 50 ºC clearly confirmed that the film was a true product of the amyloidogenic protein of αS (Figure 6 and Figure 7). Alexa-488 was attached to the C-terminal cysteine residue of a mutant form of αS, Y136C, via maleimide-sulfhydryl chemical bond formation (Figure 6A). αS-Alexa-488 gave rise to the fluorescent fibrils at 37 ºC (Figure 7A and Figure 7B) with shaking incubation. Although no protein film was found in the protein incubated at 37 ºC for 2 days, short fibrils were produced and observed with TEM. However, short fibrils could not be observed under the magnification of the confocal fluorescence microscope, so the amyloid fibril produced by shaking incubation was observed to compare the results of the same time culture. On the other hand, the fluorescent 2D film was produced at 50 ºC (Figure 7C and Figure 7D). The film formation of αS was identified as wild-type αS and Y136C mutants, and exhibited a distinct characteristic from typical fibril structures known to form αS.

## (4) Mechanism of αS specific film formation

After αS film was formed, it was confirmed that a number of αS monomer was consumed through JC-1 binding assay (Figure 8A). However, the spent αS monomer did not show the characteristic of fibril structure. Based on these

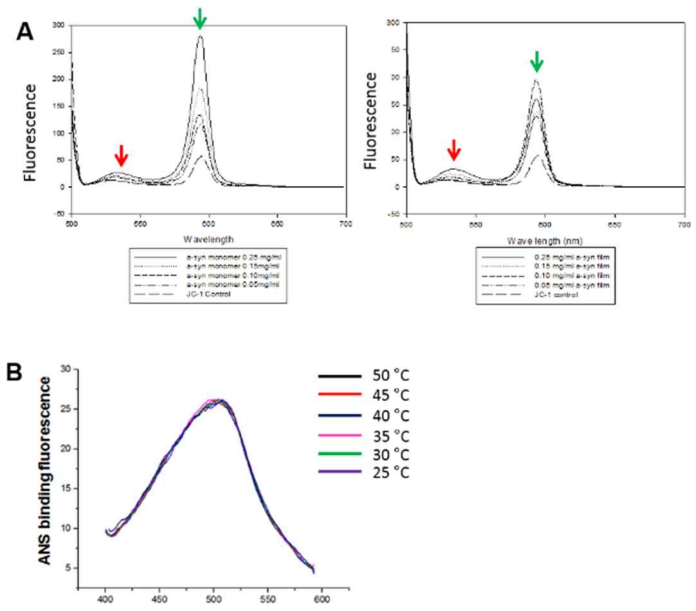


**Figure 8. JC-1 and ANS binding assay.** JC-1 binding fluorescence of αS monomers (A, left) and αS films (A, right) at various αS concentrations. (Red arrow indicates the characteristic pick of αS fibrils and the green arrow indicates the characteristic pick of the αS monomers. Experiments with ANS which is specifically react to αS structures of each temperature (B).

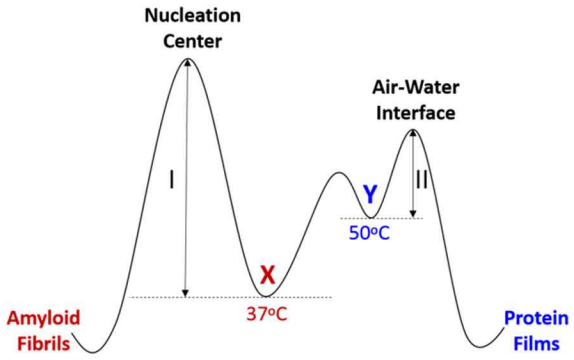


**Figure 9. Hypothetical energy diagram.** In order to explain the alternative self-assembly processes, hypothetical energy diagram was suggested about αS at 37 ºC and 50 ºC leading to the two distinctive supra-structures of amyloid fibrils and protein films.

results, it is possible to infer that αS assembled into other materials, rather than to amyloid fibrils (nanofiber), which are typical self-assembly product of αS self-assembly. Structural transition of αS to film structure, however, appeared to occur only at the interface since the ANS binding fluorescence study performed at various temperatures indicated that αS hardly changed its structure in the bulk solution (Figure 8B). The 2D assembly of αS, therefore, is considered an interface- dependent phenomenon. Since air-water interface is a reasonable environment for film formation to occur, and the αS exposed to the interface could obviously turned into a surface-active agent at 50 ºC. To explain the alternative assembly process (Figure 9), αS is assumed to exist in two undefined conformational states of X and Y at 37 ºC and 50 ºC, respectively, although both states were shown to be in mostly random state (Figure 4A). The energy level of Y which may exist in a kinetically trapped state is higher than that of X. Consequently, the conformational entropy of Y is larger than that of X, meaning that Y may have a more diverse set of conformations in equilibrium. At the air-water interface, Y shifts the equilibrium to favor an amphipathic structure leading to the protein film formation by reducing the activation energy II (Figure 9) while a structural transition of X to the amphipathic structure is hindered at 37 ºC. For the film formation, therefore, the presence of αS at the kinetically trapped state of Y at 50 ºC is suggested to be crucial since over-energization of αS at either 60 ºC or 70 ºC failed to produce the protein films (Figure 10). In the case of X, on the other hand, its local structure would form

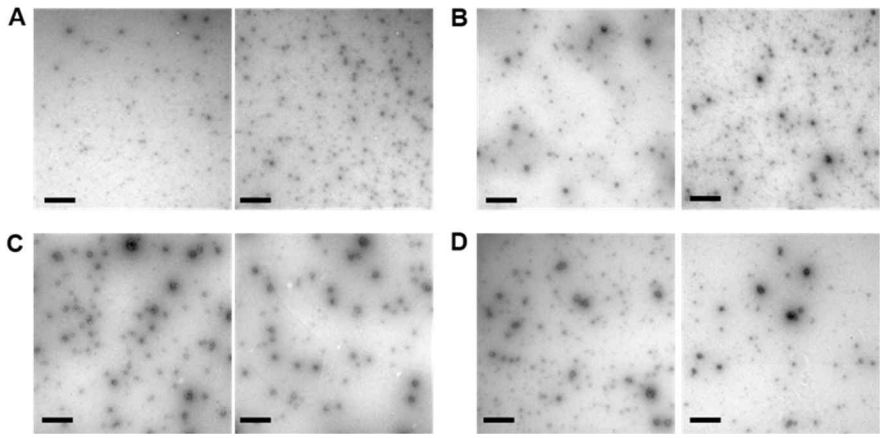


**Figure 10. TEM images of αS under incubation at higher temperatures.** TEM images of αS incubated at 60 °C (A, B) and 70 °C (C, D) for 48h (A, C) and 72 h (B, D) under a quiescent incubation. Scale bars represent 500 nm.

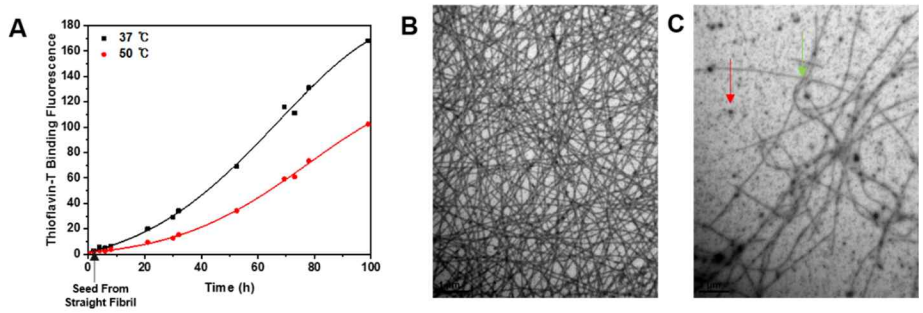


**Figure 11. Seeding effect of αS incubated at 37 °C and 50 °C.** (A) Seeding effect of αS monomers provided with fibril seed was monitored with Thioflavin-T. (B) TEM image of seeded αS morphologies at 37 °C and (C) 50 °C.

the seed during a prolonged incubation. Once the seeds develop although their seed formation is thermodynamically unfavorable, X accretes to the seeds producing the mature amyloid fibrils in the bulk solution by lowering the activation energy I (Figure 9) with a considerable conformation adjustment to the assembly-prone state. Therefore, the two separate initial states of X and Y would determine the fate of αS for the alternative assembly leading to the two distinctive suprastructures of amyloid fibrils and protein films. The 'trapped' state of αS at 50 ºC was also confirmed with other experiments. Seeding effect of αS at 37 ºC and 50 ºC was monitored with thio-flavin T assay (Figure 11). The seeding effect of αS at various temperature, the seeding effect observed at different temperatures did not show much difference from other report.[43] But in case of 37 ºC and 50 ºC, seeding effect of each temperature resulted difference of thio-flavint T binding fluorescence (Figure 11A). The TEM image of αS incubated after the addition of seeds at different temperatures showed more interesting results (Figure 11B). At 37 ºC, a typical αS straight amyloid fibrils were produced, while the αS at 50 ºC produced curly amyloid fibrils. This result makes it possible to assume that the 37 ºC and 50 ºC of αS form different outcomes from the same stimulus and exist in a dynamically distinguished state.

## (5) Optimal conditions for the αS film formation

The film formation was shown to depend on pH of the bulk solution. The 2D assembly was favored at pH 6.5 while it was hindered at either more acidic or basic conditions (Figure 12A). Ionic strength did not appear to influence the film formation since the films were still generated even in the presence of 0.6 M NaCl (Figure 12B) although non-specific protein agglomerates were also formed as revealed on the TEM image. When sucrose was employed, however, the film was optimally produced at 10% sucrose (0.29 M) (Figure 12C). This data may indicate that solution viscosity would affect the 2D assembly of αS. While suppressing molecular diffusion of αS in the bulk solution for the self-interaction, the protein could be saved for the 2D assembly at the interface. Alternatively, the sucrose could trap the protein into a certain structure favoring the 2D film formation instead of 1D amyloid fibril formation.[44-45] Unfortunately, however, CD spectroscopy failed to reveal any structural transition of the disordered structure of αS at 10% sucrose. The transient structure of αS presumably induced only at the interface did not allow its examination with conventional analytical tools besides its final assembled product of 2D films.

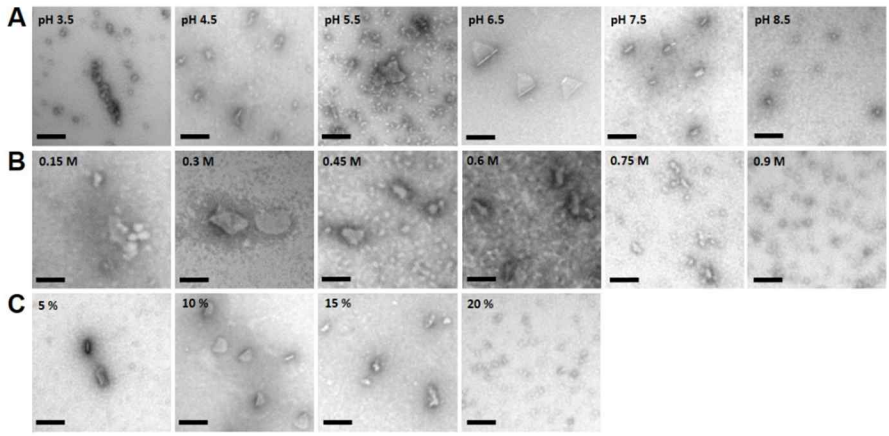


**Figure 12. αS film formation at various conditions.** (A) The αS films produced at various pHs were revealed with TEM. The αS films prepared in the presence of various concentrations of either NaCl (B) or sucrose (C) were also examined with TEM. Scale bars represent 200 nm.

## (6) Preparation of αS film at oil-water interface

The αS film was prepared at oil-water interface instead of the air-water interface in order to obtain the film which was expanded in size under the optimal condition of 50 ºC at pH 6.5. When the film was produced at the air-water interface for an extended period of time (7 days), the film was obtained in multiple layers with the height of 80-120 nm and rather a limited lateral size (Figure 13 A, Figure 13 B and Figure 14) in comparison with a single layered film of 40 nm in height obtained after 2 days of incubation (Figure 13A). On the other hand, the film prepared at the oil-water interface following 48 h of incubation increased its size by 6-7 fold over the film obtained at the air-water interface (Figure 13A and Figure 13C). Both films measured the same thickness of 40 nm. It is presumable that an amphipathic local structure of αS could be induced upon its adsorption to the oil-water interface, which would experience subsequent conformational rearrangement to exhibit stable lateral interaction leading to the 2D film formation as found at the air-water interface. The oil-water interface was therefore employed to fabricate the protein film for additional functionalization (Represented in Figure 15 compare with Figure 16).

For the film with a 40 nm thickness, it is speculated to exist in a double layered structure of the amphipathic film generated at the interface. As the films have routinely been collected in aqueous condition, the hydrophobic side would

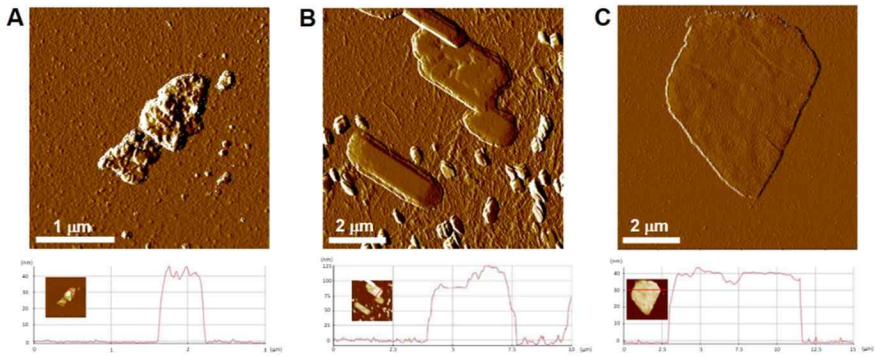


**Figure 13. αS films prepared at either air-water or oil-water interface.** The αS films obtained at air-water interface during the quiescent incubation for 2 days (A) and 7 days (B) at 50 ºC are shown in the error-signal images of AFM. Their height profiles are also shown underneath each panel with height images (inset). The film prepared at oil-water interface for 2 days at 50 ºC was also revealed with AFM in error-signal image (C) along with its height profile.

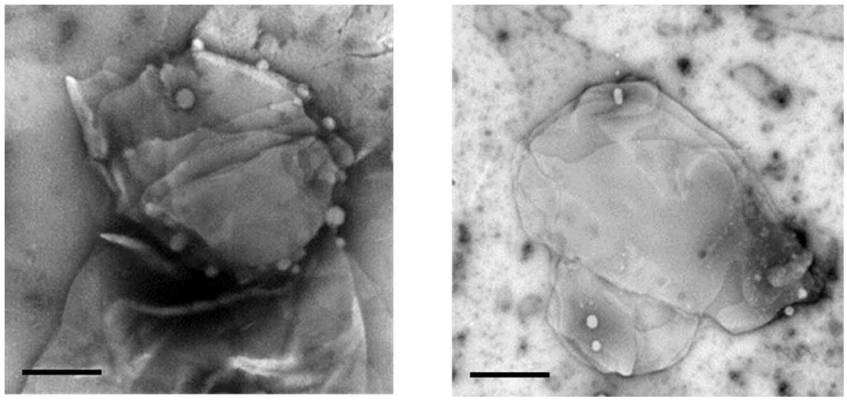

**Figure 14. TEM images of the αS films collected after 7 days of a quiescent incubation at 50 ºC.** The αS film obtained by 7 days quiescent incubation was able to confirm the stacked structure on the TEM. Scale bars represent 1 μm.

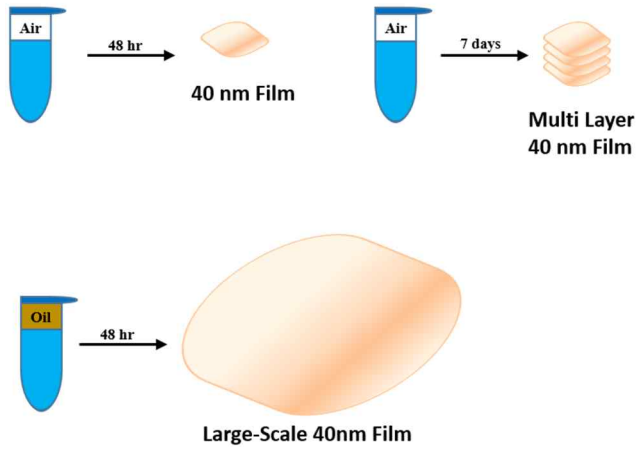


**Figure 15. Schematic representation of film formations via interfaces.** Schematic representations of film formations via αS quiescent incubation at 50 °C with air-water interface for 48hr, 144hr, and oil-water interface for 48hr.

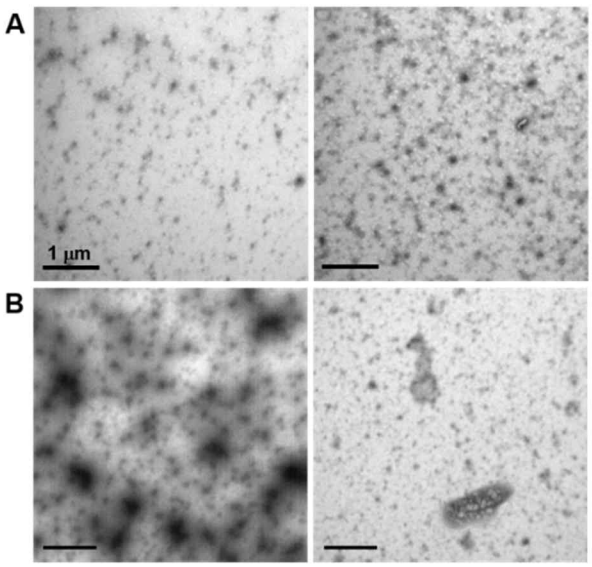


**Figure 16. TEM image of αS incubated at 37 °C with oil-water interface.**

TEM image of aS incubated at 37 °C with oil-water interface for (A) 48 hr and (B) 96 hr.

be folded up into the double-layered form to avoid its exposure to the water layer. If αS as a member of IDPs forms an amphipathic structure, the basic N-terminal segment (1-60) and the acidic C-terminal segment (96-140) could be extended like hydrophilic tails with the middle hydrophobic NAC (non-Aβ component) segment acting a head. If the longer N-terminal tail is fully extended in the amphipathic film, the length of 60 amino acids would measure 21.6 nm by considering a distance between Cα-Cα of an extended polypeptide chain 0.36 nm.[46] The proposed double-layered film, therefore, would have a thickness of 43.2 nm which is comparable to the film thickness we have obtained in this study (Figure 17).

The formation of αS film structure seems to be due to the structural features of αS. Of course, structural flexibility as an intrinsically disordered protein would have been necessary, but no film was formed using other intrinsically disordered proteins (Figure 18). In case of amyloid-β, fibril morphology was observed (Figure 18A). In the case of κ-casein, partial protein aggregates were found, but not enough to judge the film structure (Figure 18B). This difference is due to the unique structural features of αS. The distinction between hydrophilic and hydrophobic region is a common feature, but αS is the only structure in which a hydrophobic NAC region exists in the center of a protein and a hydrophilic tail is composed of both (Figure 18C). The hydrophobic interactions between the central NAC regions, which are hydrophobic, seem to

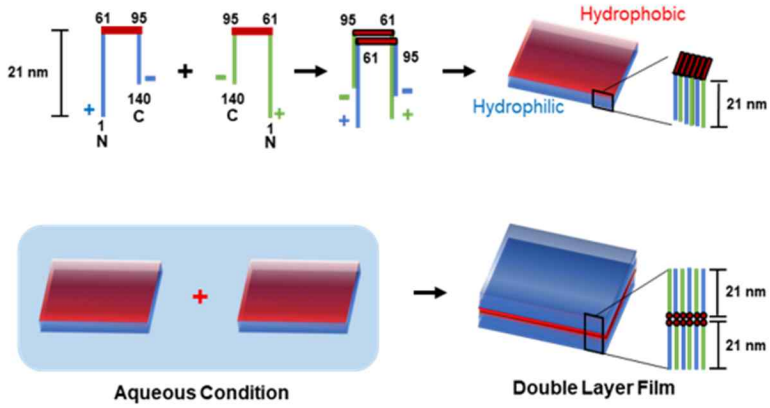


**Figure 17. Schematic representation of αS film formation.** In order to explain the formation process of αS film which shows a constant height of 40 nm, it is schematically presented based on the height that αS can form.

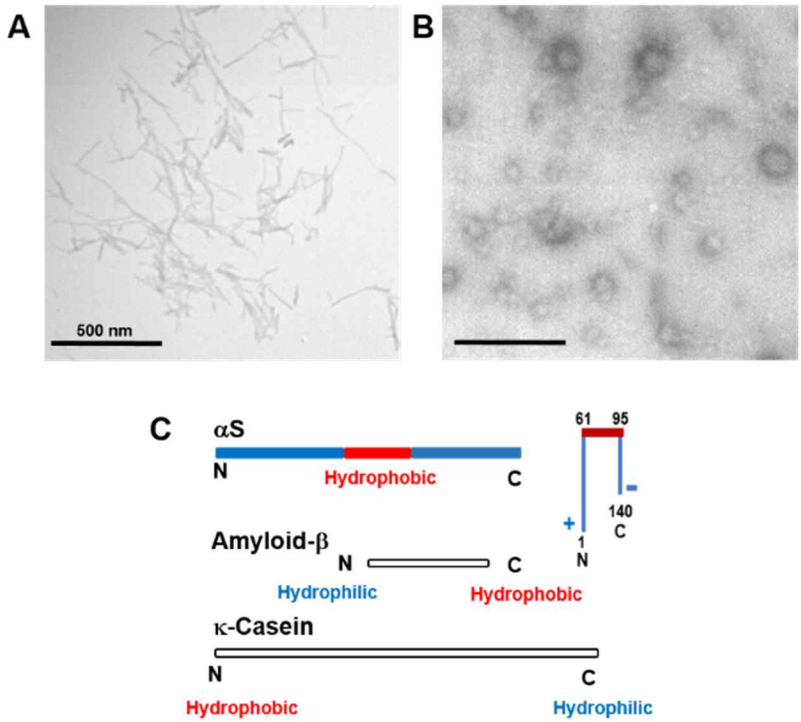


**Figure 18. IDP self-assembly at 50 °C incubation.** TEM image of amyloid-β peptide (A) and κ-casein (B) after 48 h incubation at 50 °C. (C) Schematic representation of αS and other IDP structures.

stabilize the film structure. The unique structure of αS is considered to be advantageous for causing this phenomenon. It is also confirmed that this film formation is closely related to temperature. The αS at 37 ºC showed no film structure even after a long time of 48 hr and 96 hr incubation even when the oil layer was provided (Figure 16). Thus, it was found that the formation of αS film should be accompanied by not only structure of αS, but also the structural modifications derived from the temperature provided.

## (7) Applications of αS film structure

In order to apply αS film as biomaterial, αS film was adsorbed on the glass surface. After coating with the αS film, the cells were observed to adhere on the protein film. As a result of the experiment, it was confirmed that two to three times more cells adhered to the glass (Figure 19). Along with this feature, another application was to see if it adheres to nanoparticle films. Based on previous studies, αS-AuNP film and αS-swCNT film was produced successfully (Figure 20) .[47] Observing the protein film on the nanoparticle film, the protein film was successfully adsorbed on the nanoparticle film. Based on these results, the αS film can be applied as an intercellular material for nanoparticle film or a multicellular nanoparticle film, or cell adhesion material.

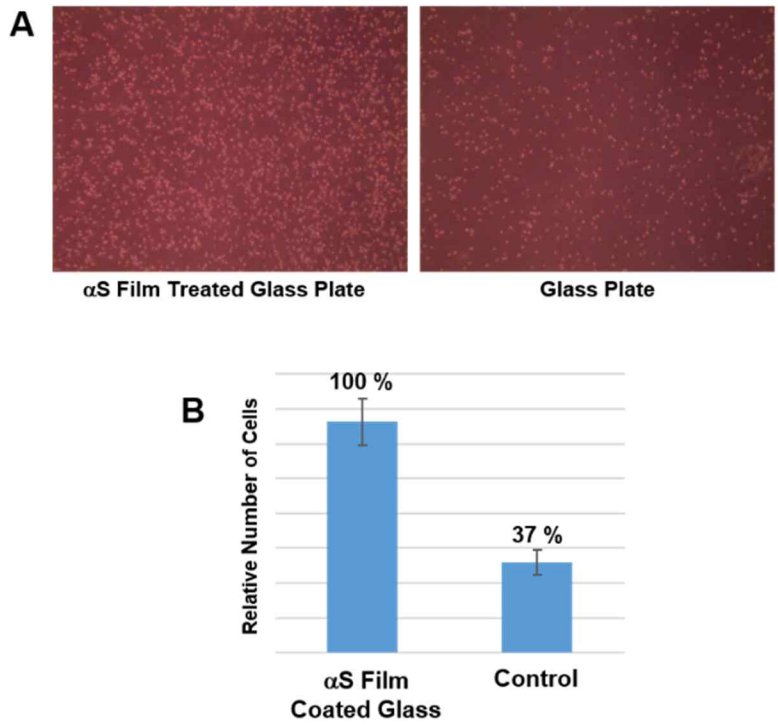


**Figure 19. αS film coating for cell adhesion.** Optical microscope image of with (A, left) and without (A, right) αS film coated glass plate after Hela cell adhesion for 1 hr. (B) Relative number of cells attached to either glass plates.

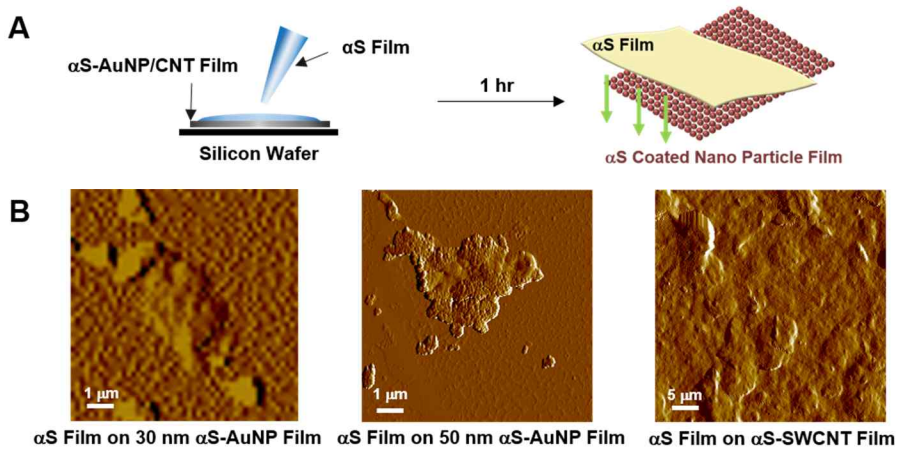


**Figure 20. αS Film Adsorption to αS-NP Films.** (A) Schematic representation of αS film adsorption to nanoparticle films. (B) αS film treated nanoparticle films were observed with AFM.

## (8) Functionalization of the αS film with PCDA

In order to secure additional applicability of αS film, a hybrid film with PCDA was employed to produce αS-PCDA hybrid film. Generally, protein films are considered a useful component to provide biological interface in the areas of drug delivery (cargo releasable patch), tissue repair and regeneration (wound dressing), cell and tissue culture, bioactive coating (implant), biodegradable film, and sensor development.[25] However, their undesirable properties such as fragility, low stability, and slow response time have limited their actual use. It was previously demonstrated that the amyloid fibrils of αS provided a template for PCDA to be aligned and photopolymerized to form the robust PDA-based colorimetric protein fibrils responding to external stimuli of heat, pH, and solvents.[48-49] In this study, therefore, PCDA was also employed to be integrated onto the αS film in order to improve its functionality. The resulting PDA-based protein film was expected to exhibit augmented physical and chemical stability, electrical conductivity, optic property showing colorimetric blue-to-red transition responding to the stimuli.

PDA materials are based on the conjugated polymer system exhibiting useful optical properties distinctive from other sensing systems.[50-51] Molecular alignment of diacetylenes and subsequent facile photopolymerization with simple UV irradiation in the absence of any catalysts are required for the

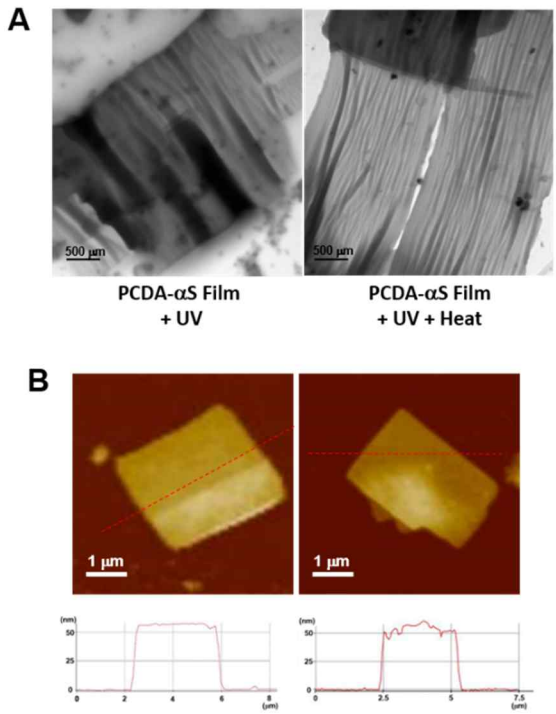


**Figure 21. TEM and AFM images of PCDA immobilized αS films.** (A) TEM images of the PCDA immobilized αS films after UV irradiation in the absence (left) and presence (right) of subsequent heat treatment. (B) AFM images of the PCDA-αS films obtained via UV irradiation before (left) and after (right) the heat treatment at 80 ºC are shown in the error-signal images. Their height profiles are also shown with height images (inset).

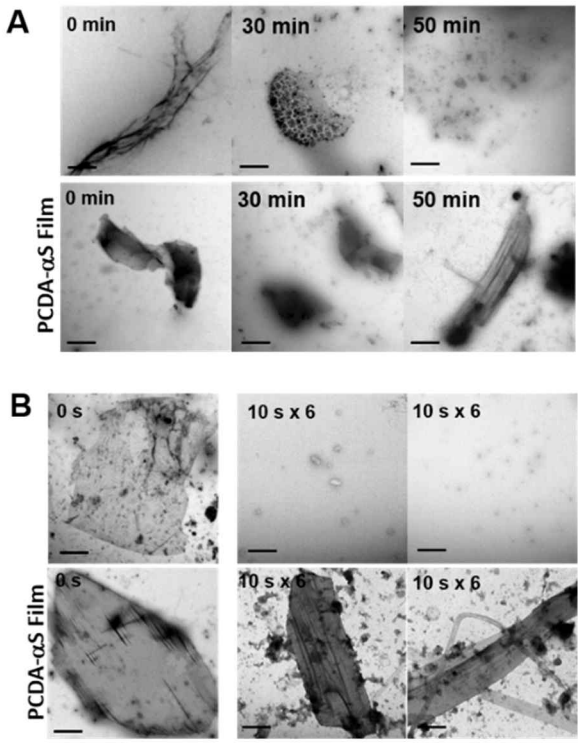


**Figure 22. Stability of PCDA-αS film.** (A) TEM images of the αS films (top) and hybrid PCDA-αS films (bottom) are compared following the trypsin-treatment for the durations indicated (B) and after the sonication with 10 s/cycle for 6 cycles (D).

conjugated polymerization yielding blue color.[52] Its colorimetric transition to red color is sensitive to not only environmental stimuli such as temperature, pH, and organic solvents, [53-55] but also biological agents including pathogenic bacteria, viruses, and proteins.[56-58] Its usefulness arises as the color transition has been routinely detected with the naked eye. The red color could also be monitored with a fluorescence-detection system.[59] However, since the PDA-based sensor system has been usually prepared in either liposomes or films, their intrinsic structural vulnerability to mechanical stress or any disruptive chemical agents needs to be overcome by producing more mechanically robust and chemically stable sensor system.[60-61] In that respect, PCDA-αS hybrid film system has been demonstrated to have several advantageous points over the poly-PCDA vesicle system. In solution, both systems responded equally well to the stimuli such as temperature, pH change, and ethanol although the poly-PCDA vesicles showed a faded color change with ethanol due to the vesicular instability in the solvent.[48] On the solid surface of filter paper, however, the poly-PCDA vesicles were not able to detect those external stimuli since their structural intactness was seriously affected upon their contact with the paper.[49] On the other hand, the PCDA-embedded αS films immobilized on the surface have been shown to respond readily to the stimuli including various solvents. In addition, the final red phase could be quantitatively monitored by detecting its emitted fluorescence or the electric conductivity of the hybrid films placed on the surface of silicon wafer. Moreover, the PCDA integration not only

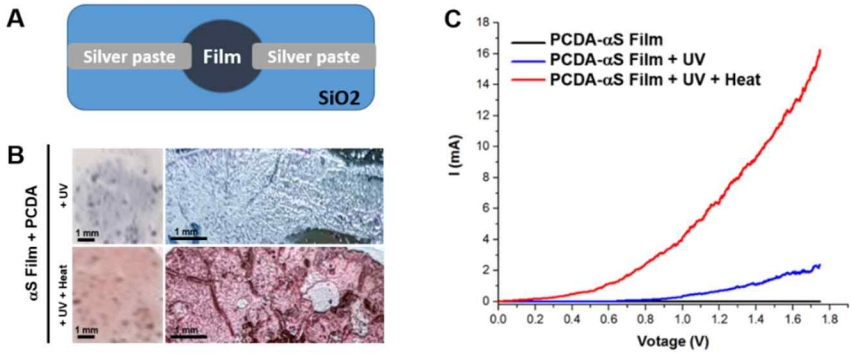


**Figure 23. Colorimetric transition of the PCDA-αS films and their electrical conductivity.** (A) Schematic representation of preparing SiO2 wafers to examine electrical properties. (B) Optical images of the PCDA-αS hybrid films irradiated with UV before (top) and after (bottom) the subsequent heat treatment. The hybrid films were examined on top of either filter-paper (left) or $SiO_2$ wafer (right). (C) IV-curves to monitor conductivity of the PCDA-αS films before (black line) and after (blue and red lines) the UV irradiation in the absence (blue line) or presence (red line) of the subsequent heat-treatment.

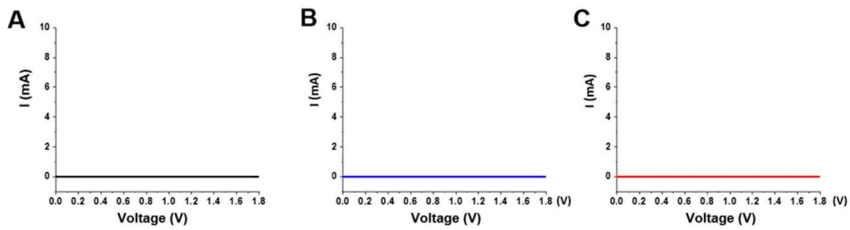


**Figure 24. IV curves of the PCDA treated amyloid fibrils of αS.** IV curves of the PCDA-αS amyloid fibrils in the absence (A) and presence (B) UV irradiation with additional heat-treatment (C).

strengthens the protein film but also makes the resulting hybrid film resistant against proteolysis.

The αS film obtained at the oil-water interface was subjected to the PCDA treatment at 1 mM for 2 h at room temperature. The PCDA-αS hybrid films were irradiated with UV at 254 nm for 10 min followed by a heat treatment at 80 ºC for 3 min. Regardless of the heat treatment, the PCDA-αS hybrid films appeared denser than the αS films prepared without PCDA as revealed with TEM (Figure 21A). Introduction of PCDA raised the thickness of αS film by 12-15 nm as evaluated with AFM (Figure 21B). The PCDA integration was demonstrated to provide the hybrid film with chemical and physical stability as assessed with trypsin digestion and sonication. While the αS film was completely degraded by trypsin at 0.1 mg/mL after 50 min, the PCDA-αS hybrid film after the UV and heat treatments was hardly affected by the enzyme (Figure 22A). The PCDA-αS hybrid film was also shown to be mechanically robust since the film was not disrupted by tip-sonication at 20 kHz under 750 W (10 s x 6 times) whereas the αS-only film was completely disintegrated (Figure 22B).

The PDA-based colorimetric transition of the fortified αS film was also examined. After an extensive wash with water, the PCDA-αS hybrid films localized on a filter paper were exposed to the UV followed by the heat treatment, which gave rise to blue to red color transition, respectively

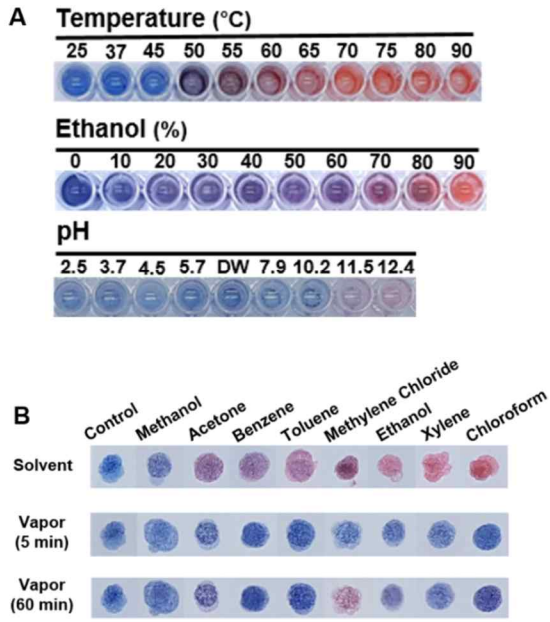


**Figure 25. Colorimetric transition of the PCDA-αS films.** (A) Colorimetric response of the PCDA-αS films to temperature, ethanol, and pH. The photopolymerized hybrid films present in solution at blue state were subjected to the stimuli at various extents as indicated. (B) Colorimetric transition of the PCDA-αS films immobilized on a filter paper at blue state to red in the presence of the solvents and their vapors.

(Figure 23A, left). The blue-to-red transition was also observed for the PCDA-αS hybrid films adsorbed on the surface of $SiO_2$ wafer (Figure 23A and Figure 23B). Intriguingly, the PCDA-αS hybrid film was found to be electrically conductive only at the red film state, not the blue state, indicating that the PDA rearrangement induced by the heat treatment on the photopolymerized PCDA permitted the transition of electrons through the molecular network (Figure 23C). In addition, these data indicate that a structural regularity required for PCDA to be localized and photopolymerized on the film would be distinctive from the β-sheets of αS amyloid fibrils which were also demonstrated to serve as a template for the PCDA immobilization producing active PDA-materials[49] since the films were found to be lacking in the β-sheet structure (Figure 4). In addition, the amyloid fibrils conjugated with PCDA did not show any conductivity even after the colorimetric transition to red state with the UV and heat treatments (Figure 24). In the previous report, the red state of PDA reported that the electrical flow was not smooth due to its surface characteristics such as roughness and crack development.[62] However, the PCDA film formed with αS film showed higher electrical conductivity in the red state. From these results, αS film not only acted as a scaffold for the polymerization of PCDA, but also affected the structural characteristics of PCDA film and contributed to the expression of new physical properties.

Nevertheless, this hybrid film was also responsive to the external stimuli such as temperature, pH, and solvents (Figure 25A and 25B) as observed with

the PCDA immobilized amyloid fibrils. The blue-to-red color transition of the films present in solution started to occur from 55 ºC, pH 11.5, and 70% ethanol (Figure 25A). In addition, the solvents such as methanol,acetone, benzene, and toluene could be discriminated from the other ones such as methylene chloride, ethanol, xylene, and chloroform with the color change of the hybrid films immobilized on a filter paper as they were directly exposed to the solvents. With the vapor, methylene chloride was the only solvent which gave rise to the color transition after 60 min of the exposure (Figure 25B). Based on these characteristics, therefore, this PCDA-αS hybrid film could be considered to play a dual role of both colorimetric and electric sensor toward the environmental stimuli.

## (9) Additional applications of αS film

From the properties of the αS film presented above, αS film can be used as various biocompatible scaffolds or materials (Figure 26). The interaction with nanoparticle films and the biocompatible properties seen in cell adsorption experiments suggest their applicability as surface functionalizing materials containing substances such as enzymes and drugs.[63] αS film itself may have applicability. According to previous reports, protein films having a height of

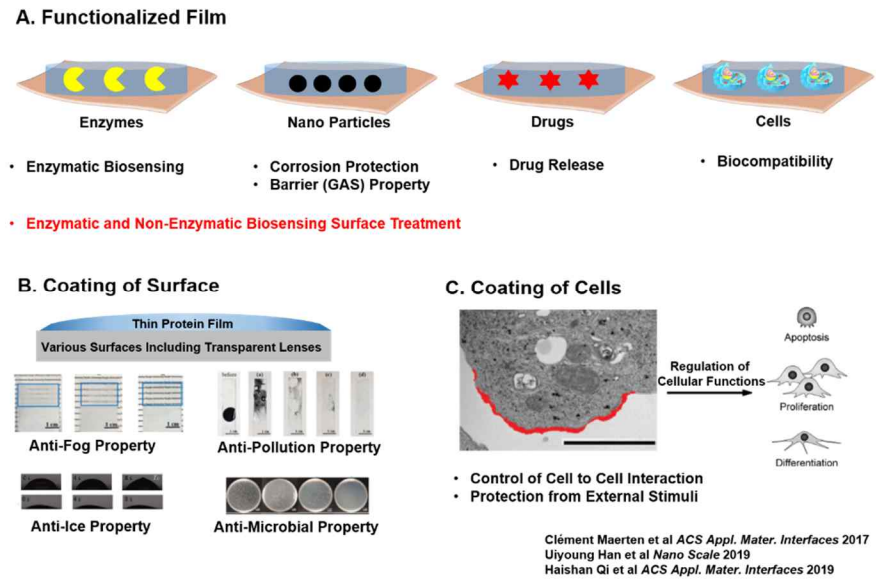


**Figure 26. Additional applications of αS films.** (A) αS films can be used for surface treatment containing nanoparticles or cells, additional treatment of nanoparticle film, and application as an intermediate material (Clément Maerten et al *ACS Appl. Mater. Interfaces* 2017). (B) αS film having a height of 40 nm can be applied to the surface treatment by applying to a transparent lens or film (Uiyoung Han et al *Nano Scale* 2019). (C) αS film can be applied to control of differentiation resulting from partial coating of stem cells (Haishan Qi et al *ACS Appl. Mater. Interfaces* 2019).

nanometers can be given additional properties by coating a transparent lens or membranes.[64] The biocompatible features of protein films could also affect stem cell differentiation. Recent reports have shown that localization can also be controlled by partial protein-based coating of stem cells.[65]

# I-3. Conclusions

Based on the contents of Part I, conclusion follows (Figure 27).

1. αS protein film was prepared with αS monomers, a protein which structure is not defined in the monomer state.

2. αS film was produced through a 50 °C quiescent incubation.

3. Formation of the αS protein film was confirmed through the incubation of αS Y136C mutant.

4. Structural differences were observed but the major component of αS film structure was random structure, suggesting film formation process was performed at the water-air interface.

5. αS film was applied as an effective material for cell adhesion, and showed applicability as an intermediate or coating agent to nanoparticle films.

6. By providing oil-water interface, it was possible to produce a film that was 7,8 times larger than air-water interface.

7. PCDA-αS hybrid film was successfully polymerized, and showed different colors via various external stimuli, and confirmed the electrical conductivity difference due to thermal stimulation.

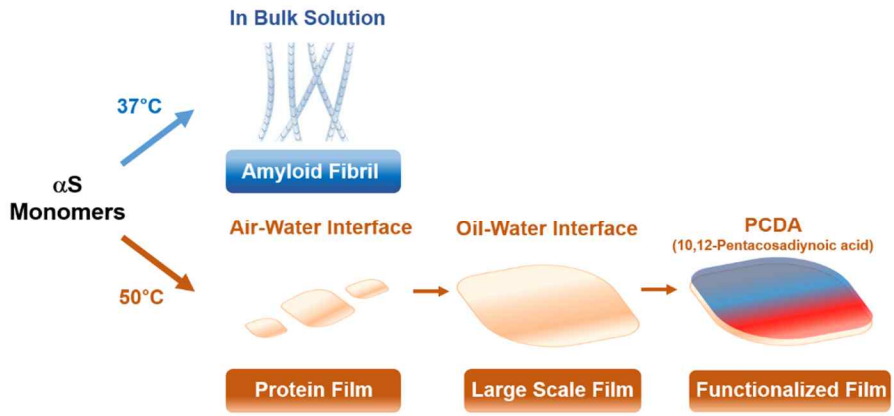


**Figure 27. Conclusion Part I.** Schematic representation of αS film formation based on alternative self-assembly of αS and modification of film with PCDA.

# Part II.

# Fabrication of α-Synuclein Microspheres and its Applications

## II-1. Introduction

### (1) Structural plasticity of αS oligomers

αS oligomers are structurally flexible**.** The structural flexibility of the oligomers can be demonstrated without having to build on the fact that the oligomers are based on structurally flexible, intrinsically disordered αS monomers. In fact, the oligomeric species of amyloidogenic proteins have been suggested to act as either a nucleation center for the template-dependent fibrillation[66-67] or a growing unit in the template-independent process as observed with the self-assembly proteins of αS, amyloid-β, and κ-casein[68-69]. It may be helpful to refer to data obtained from small angle neutron scattering (SANS) analysis of αS oligomers.[70] αS oligomers incubated at different temperatures were prepared in deuterium for neutron scattering measurement.

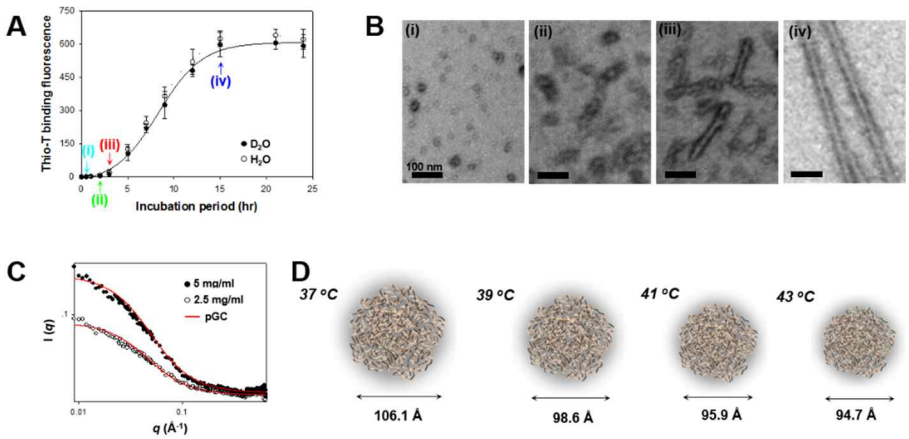


**Figure 28. Diversity of αS oligomers. (**A) The growth curve under deuterium is well represented by sigmodal curve. (B) The characteristics at each growth curve point were also represented. The best results were obtained when fitting pGC model. By calculating the size of each oligomer based on the fitting values, diversity of the size of each oligomer were confirmed.

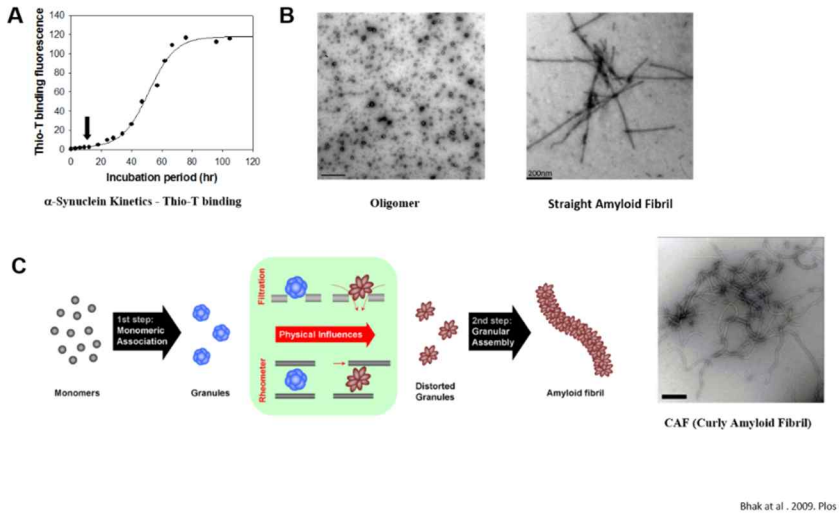


**Figure 29. Structural plasticity of αS oligomers**. (A) Oligomers can be obtained where growth curves do not yet exhibit β-sheet structure. (B) Generally, oligomers form linear amyloids through additional self-assembly. When the physical stimulus is continuously applied to the oligomer, the oligomer forms a tortuous curved amyloid fibrils (C).

αS growth curves produced excellent sigmoidal curve, even in deuterium, as in normal 20 mM MES buffer (Figure 28A). The measurement of the TEM to confirm the protein structure at each point shows the distribution of oligomer-short fibrils-long fibrils (Figure 28B). Based on the measured scattering, the poly-Gausian Coil (pGC) model showed the highest fitting coefficient (Figure 28C). Analysis of the oligomers with the pGC model shows that αS oligomers have distinct sizes depending on the temperature at which they are prepared (Figure 28D). Structural flexibility of the oligomers is not only visible, but can also be observed in the differences in the final structure of self-assembly. In the previous report, it was confirmed that when physical stimulation was applied to the same αS oligomer under the same culture conditions (Figure 29), it formed a structure of a curved amyloid fiber (CAF) rather than a linear amyloid generally observed (Figure 29B and Figure 29C).[15] The CAF structure was formed by applying a constant physical stimulus to the oligomer using a pore size smaller than the oligomer based on the centrifugal membrane filter (Figure 29C). Based on these results, the oligomer has structural flexibility, and it can be seen that there is a difference in the final conjugate of self-assembly by using an external stimulus.

## (2) Sphere structures in engineering

Spherical structures have applicability in various ways (Figure 30). Basically, the spherical structure is attracting attention in various fields such as pharmaceutical, agriculture, beauty and food based on its structural characteristics.[71] However, previous studies clearly show limitations in the formation process or structural character. The first example is to make spherical structures by making various solution compositions on spider silk protein. Proteins were spherically formed by self-linking the silk fibroin protein at various pH conditions (Figure 30).[72] The spherical structures were induced by the self-bonding of proteins, but the formation conditions are formed at too low pH, and their formation is reversible, which presents a problem of limitation in applicability. Another form of protein spheres was achieved by controlling the freezing point (Figure 30).[73] Although the constituent proteins are self-assembly proteins and proteins were also have amyloidogenic properties, the spherical structures formed were very unstable at room temperature and require further chemical treatment such as harsh cross-linking. The spherical structure reported in another study was fabricated in its inner form and had a limit of applicability.[74] In this study, we fabricated a spherical structure based on its own self-assembly that is stable at room temperature without additional chemical treatment and can induce additional self-assembly.

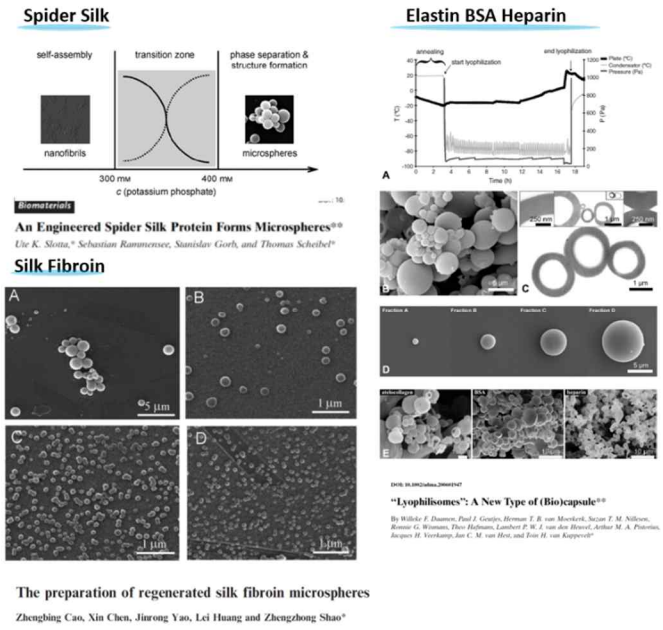


**Figure 30. Research trends in protein based microspheres.** (A) Spider silk protein form microspheres under low pH value **(***Ute K. Slotta et al. Angew. Chem. Int. Ed. 2008*). (B) Silk fibroin protein self assembles to microspheres (*Zhengbing Cao et al. Soft Matter, 2007*). (C) Microsphere formation via controlling freeze temperature and freeze drying (*Willeke F. Daamen et al. Adv. Mater. 2007).*

# II-2. Results and Discussions

## (1) Microsphere formation of αS

αS oligomers were prepared and separated for microsphere fabrication (Figure 31) (for αS oligomer details, please see the experimental part of this report). The αS microsphere structure was made in three stages. freezing, annealing, freeze drying. First stage was freezing under fast cooling rate. Rapid cooling generally refers to a condition of temperature change of more than 10 degrees per minute, and microspheres are manufactured using liquid nitrogen. Through this rapid cooling process, ice crystals are formed simultaneously, there is a limit to the growth of ice crystals, and the super concentration of protein is made up of very small portions.[75] These environments maximize the surface area of protein and ice contact. On the other hand, slow cooling process, only a few ice crystals are produced and frozen in such a way that they grow. Proteins are pushed out by growing ice crystals, resulting in a cluster of highly concentrated proteins in the middle of the solution. The difference in freezing speed was found to be one of the key factors in the production of microspheres from experimental data. When the other factors differ only in the rate of freezing of the oligomer in the same controlled state, the rapid cooled αS

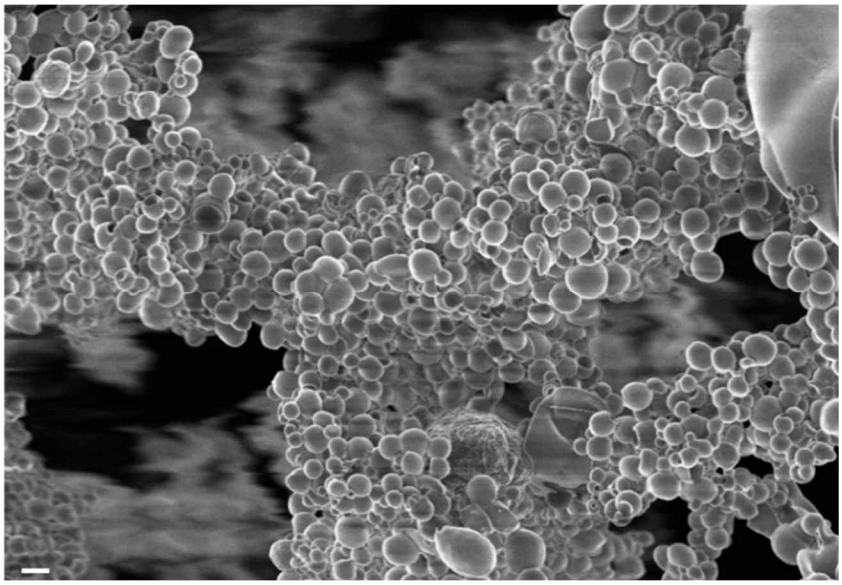

**Figure 31. Formation of αS microspheres.** Microspheres from αS oligomers were fabricated through 3 steps. Rapid cooling, frozen annealing and freeze drying. Fabricated microspheres were observed with SEM. Scale bars represent 2μm.

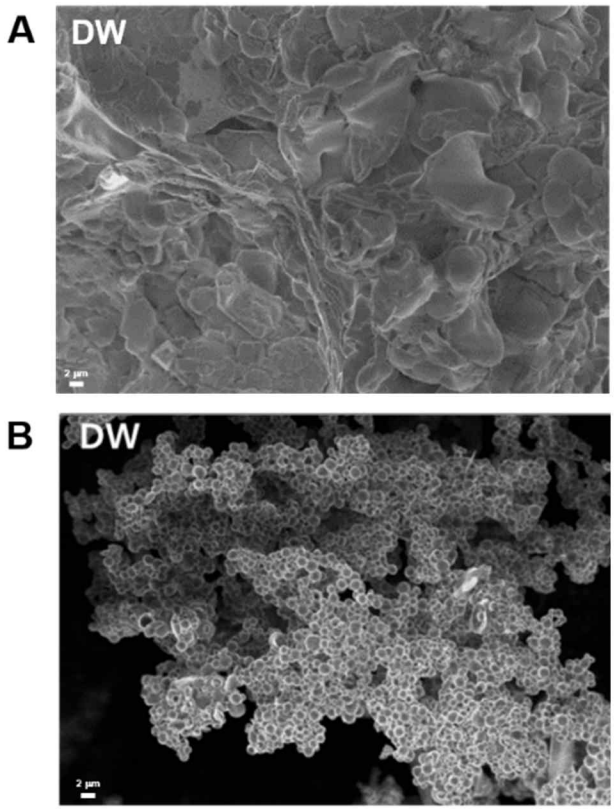


**Figure 32. Microsphere formation difference with cooling rate.** SEM image of protein aggregates formed at slow cooling condition (A) and microsphere structures formed at rapid cooling (B).

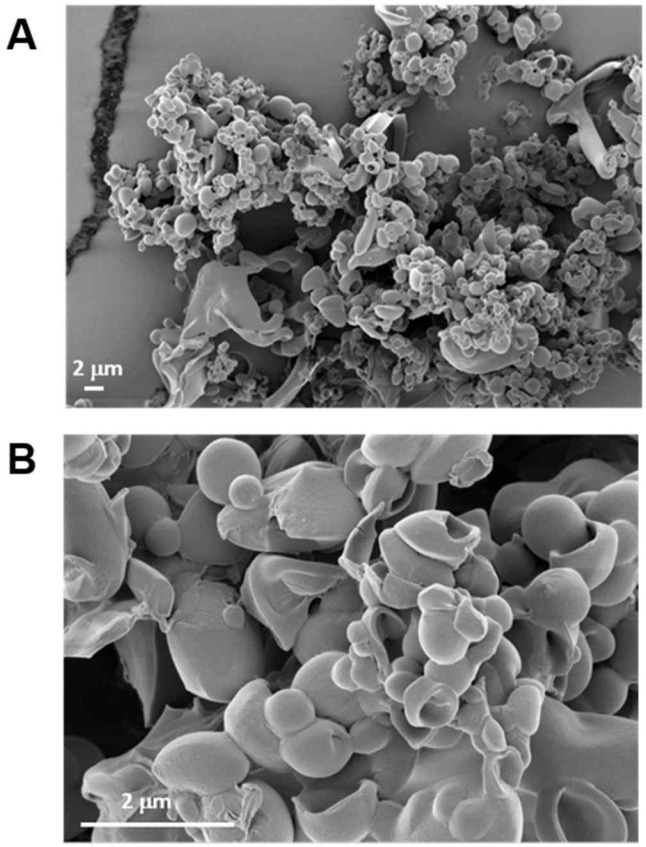


**Figure 33. Microsphere formation without frozen annealing.** Low magnification (A) and high magnification (B) SEM images of αS without frozen annealing.

oligomers formed fine microspheres (Figure 32B), whereas the protein aggregates partially identify the slow cooling αS oligomer showed no sphere structures (Figure 32A).

The second step is frozen annealing step. Frozen annealing affected the morphological integrity of the microspheres. Under the condition that the freezing duration was 5 h or more, it was possible to produce a spherical structure having a shape without a hole and having a uniform distribution uniformly in size (Figure 34). The frozen annealing was examined at three temperatures. The solution was kept in 0 °C, -20 °C and -80 °C (Figure 35). 0 °C is a condition where the structure of the ice completely collapses and the boundary between the solute and the solvent disappears completely. Microspheres which was annealed at 0°C, showed uneven shape, such as severe unevenness and a hole in the spheres. -20 °C is known as the temperature at which the ice begins to partially melt. The ice structure does not completely collapse at this stage, but it is partly a condition where the ice structure begins to collapse.[76] After -20 °C frozen annealing stage, the spheres formed more clearly than at 0°C, but the non-uniformity of the spheres was still observed. Microsphere formation was best observed after -80 °C frozen annealing stage. The -80 °C condition is the temperature reported to produce Quasi liquid layer (QLL) on the ice surface (Figure 35).[77] The appearance of QLL layer starts at -80 °C with thickness about 5 nm, and the thickness increases with increasing temperature. The temperature -80 °C is the temperature that is maintained in

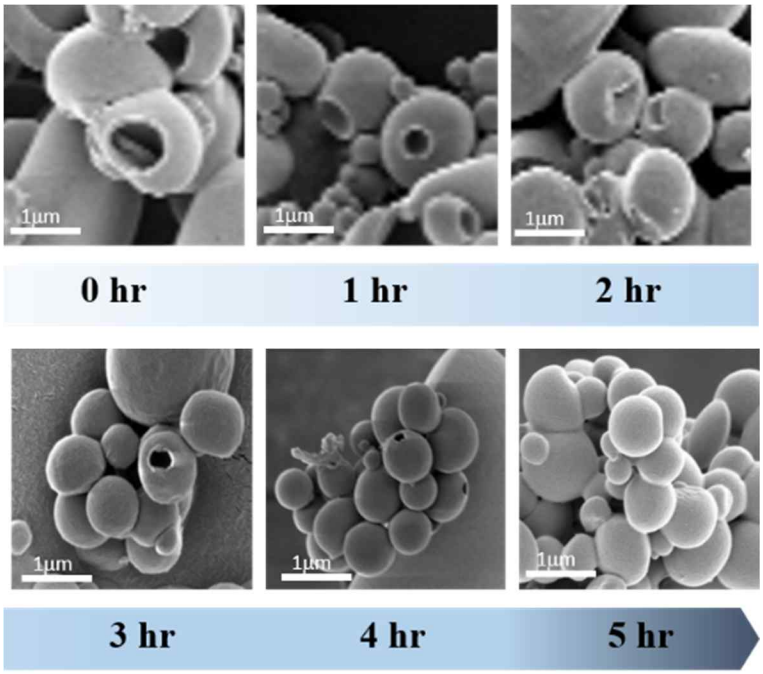


**Figure 34. αS microsphere formation with frozen annealing time difference.**

SEM images of αS microspheres followed by frozen annealing time at -80 ℃

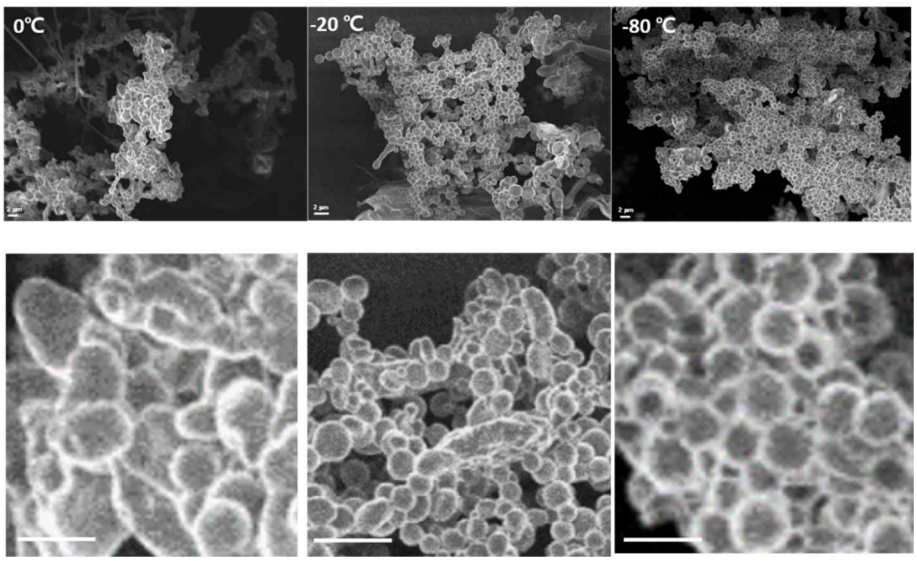


**Figure 35. αS microsphere formation with different annealing temperatures.** SEM images of αS microsphere formation with different frozen annealing temperature 0 ℃ (left), -20 ℃ (center), -80 ℃ (right).

the glassy state, not the crystal state which every molecule is frozen, in the position of αS in the aqueous solution.[78]

Finally, the third step is the freeze drying process. The freeze drying process of frozen aqueous solution in which protein is dissolved can be divided into two phases that is primary drying and secondary drying.[79] In primary drying phase, the bulk ice crystals that is not bound with protein molecules sublimate rapidly. In contrast the secondary drying phase which is much slower than the primary phase sublimation can be divided in to two systems. One is sublimation of bounded water molecules which exist to ice crystals surrounding partially highly concentrated αS. Another secondary drying is evaporation of water molecules bound to proteins. It is very important to remember the ‘glass state’ of protein-water molecule at -80°C. This evaporation induces a coffee staining effect (Figure 36), which is closely related to the structure of αS microsphere. Coffee staining effect (Coffee ring effect) is a phenomenon in which evaporation takes place at the end of the drop rather than in the middle of the drop, in three dimensions, more actively at all 'ends'. One kind of this evaporation method has been reported previously under the name of ‘lyopilisomes’[73], but the principle presented in this study is based on the theory of glass state based on the protein-water molecule combination, rather than directly controlling the melting point. The size of the prepared microspheres was controllable according to the concentration of incubated oligomers of αS (Figure 37).

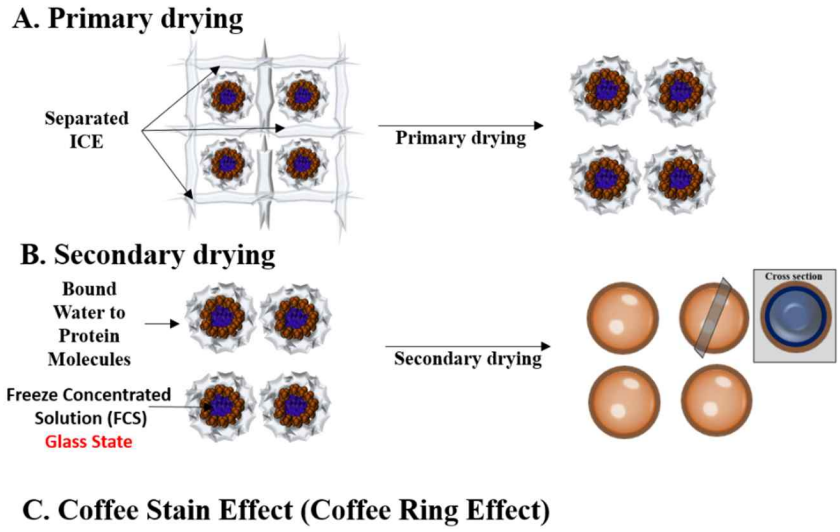


**Figure 36. Three steps of freeze-drying of αS oligomers.** Schematic representation of freeze drying process. (A) Primary drying, (B) Secondary drying and (C) Evaporation process with coffee stain effect.

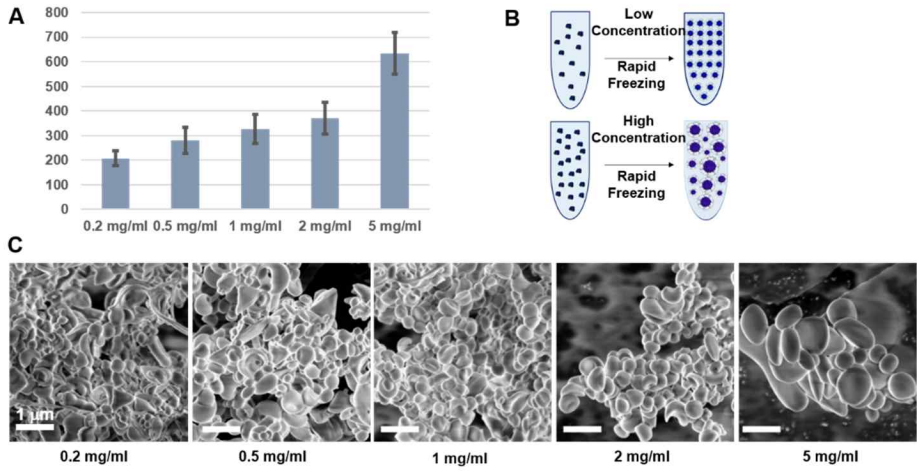


**Figure 37. Size distribution of αS microspheres based on αS concentrations.**

(A) Size distribution of αS microspheres of different concentration of αS. (B) Schematic representation of freezing conditions under different αS concentration. (C) SEM image of αS microspheres of each concentration of αS.

## (2) Structural features of αS microspheres

In order to observe the inside information of the αS microspheres, eosin that reacts specifically to αS was treat to αS oligomers (Figure 38). After 1h reacting with αS oligomer and removing the remaining eosin, the same process was carried out to produce microspheres. αS-eosin microspheres were dissolved in water again and z-stack tomography with fluorescence microscope revealed that the structure was empty inside that is 'hollow' structure (Figure 38). Partial cutting experiments using focused ion beam (FIB) attached to the scanning electron microscopy (SEM) also confirmed that the inside of the structure was an 'hollow' structure (Figure 39).

## (3) Secondary structure measurement of αS microspheres

Attenuated total reflectance-fourier transformation infrared spectrophotometer (ATR-FTIR) was measured to determine the structural state of the proteins constituting the microspheres. The FTIR data showed that the αS constituting the microspheres were partially in β-sheet structures (Figure 40). The results of the fluorescence reaction using thioflavin T, which is known to specifically react on β-sheet structure, also support the FITR data. The experimental results

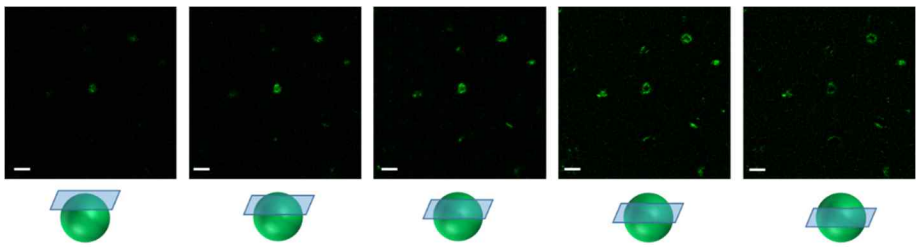

**Figure 38. Confocal microscopy of αS-eosin microspheres.** z-stack images of αS microspheres fabricated with αS-eosin complex. Scale bars represent 2μm.

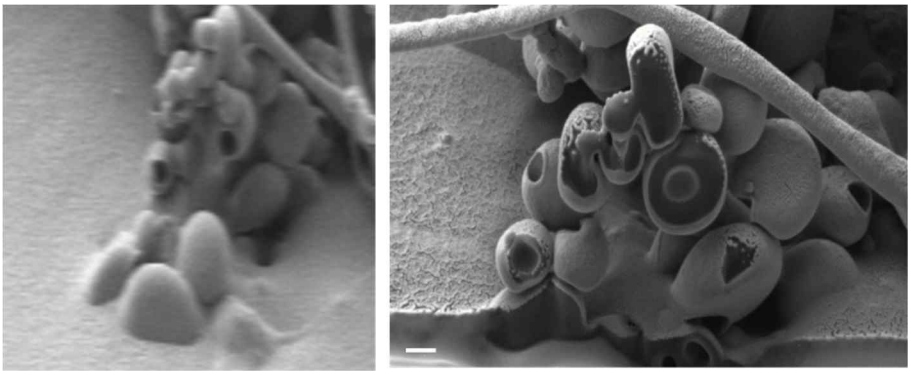

**Figure 39. SEM images of αS microspheres cut with focused ion beam.** SEM images of αS microspheres before (left) and after (right) focused ion beam treatment. Scale bar represent 200nm.

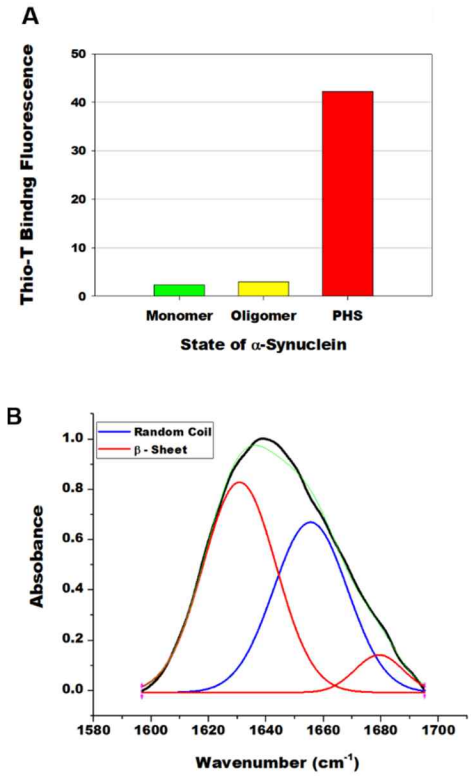


**Figure 40. Protein secondary structure analysis of αS microspheres.** Secondary structure of αS constituting microspheres. (A) Thioflavin-T binding fluorescence and (B) FTIR

showed that the αS microspheres had higher content of β-sheet structures than those of monomers and oligomers, which were relatively lower than those of αS amyloid fibers. This result, which does not fully express the potential for the β-sheet structure of αS molecules, presents two possibilities. When oligomer structures that did not have structural features (random structure) were converted to β-sheet based on a series of stimuli, non-β sheet oligomers could be converted to other structures, or additional structural transformations would be possible if all oligomers had to be β sheet structures. Considering that no other peaks were observed through FTIR structure analysis and no structural change to α-helix was observed through CD data, it was concluded that these microspheres were structures that could be further transformed to additional self-assembly.

## (4) αS microsphere stability in water

The microsphere structure was observed to be stable for more than 2 h when re-dissolved in water (Figure 41). This was a very noteworthy phenomenon. The previously reported protein-based microcapsules do not have stability when re-dissolved in water, requiring an additional cross-linker. The use of such chemical cross-linkers is fatal to the materials used, but it also poses a major

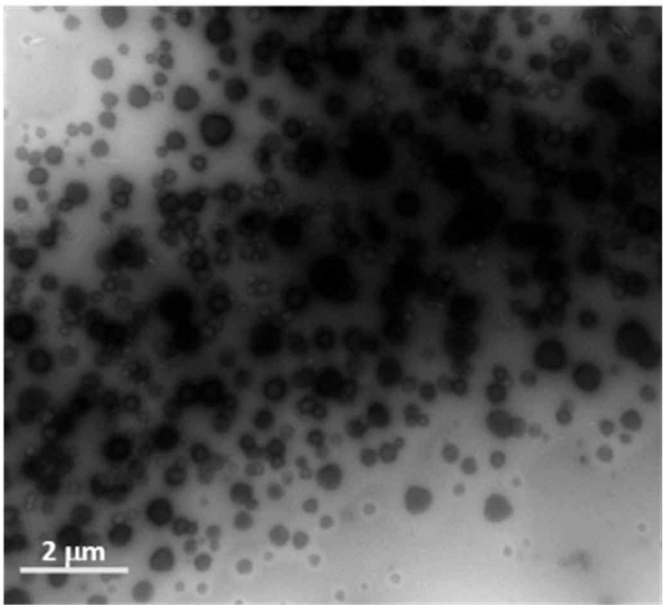


**Figure 41. αS microsphere structure stability when re-dissolved in water.**

TEM image after 2 hours of αS microspheres re-dissolution in water.

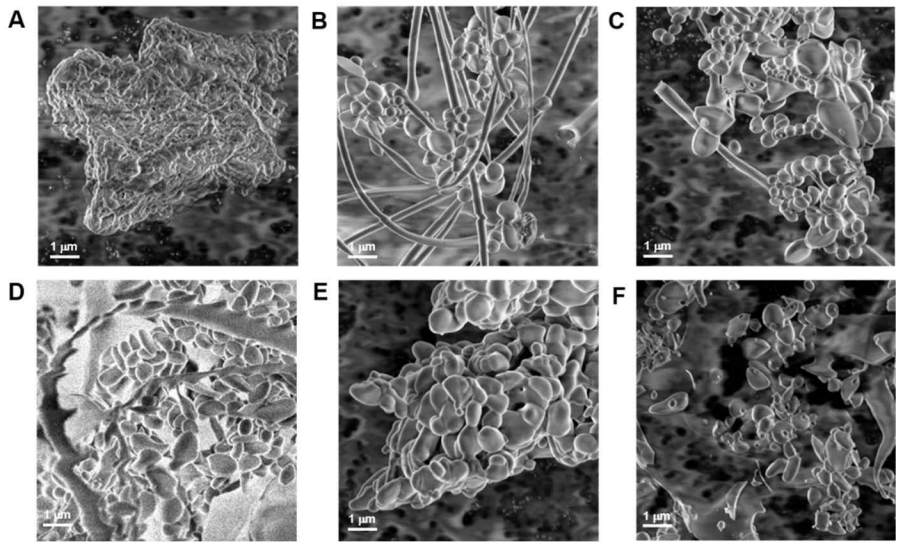


**Figure 42. Protein microsphere formation of other proteins.** SEM image of protein microspheres of (A) amyloid-β (1-40) peptide, (B) κ-casein, (C) α-lactalbumin, (D) β-lactoglobulin, (E) BSA and (F) lysozyme.

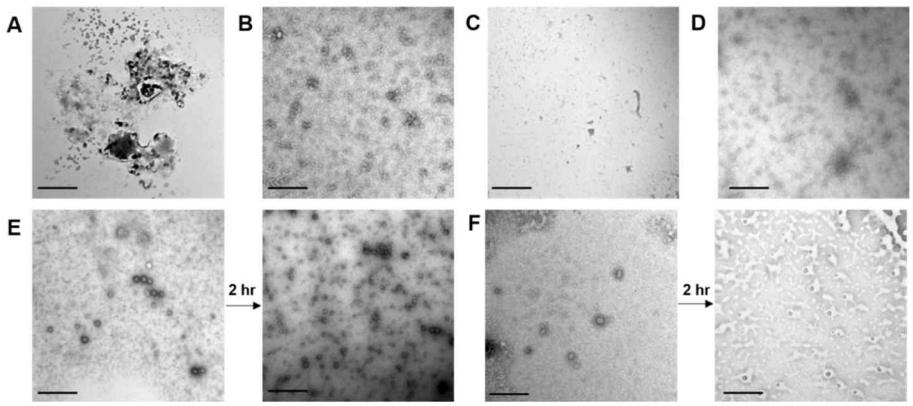


**Figure 43. Stability of microspheres derived from other proteins.** TEM image of microspheres of (A) amloid-β (1-40) peptide, (B) BSA (C) β-lactoglobulin (D) α-lactalbumin (E) κ-casein and (F) lysozyme after resolved in water. (Scale bars represent 1 μm)

obstacle to the application of the capsules or spheres. This stability of the αS microspheres has significant implications for its applicability, probably based on the β-sheet structure identified in the structural analysis data. Using other proteins, the construction of spherical structures from lyophilized samples could be confirmed (Figure 42). This result shows that the three-step αS microsphere fabrication principle may contribute in part to the fabrication of other protein spherical structures. However, in order to ensure structural stability when dissolved in water, the binding between proteins must occur. This phenomenon was not observed in experiments using other proteins (Figure 43).

## (5) Amyloid bur assembly

## (5-1) Amyloid bur formation of αS microspheres

In order to determine whether additional self-assembly of αS microsphere is possible, experiments were carried out on the possibility of additional assembly on 20 mM pH 6.5 MES buffer. First, αS microspheres prepared according to the experimental procedure introduced above were gently melted onto the 20 mM pH 6.5 MES buffer. After incubation 24 h at 37 degrees with αS microspheres as a quiescent incubation, the morphology similar to chestnut bur so called amyloid bur structure was assembled (Figure 44A and Figure 44B).

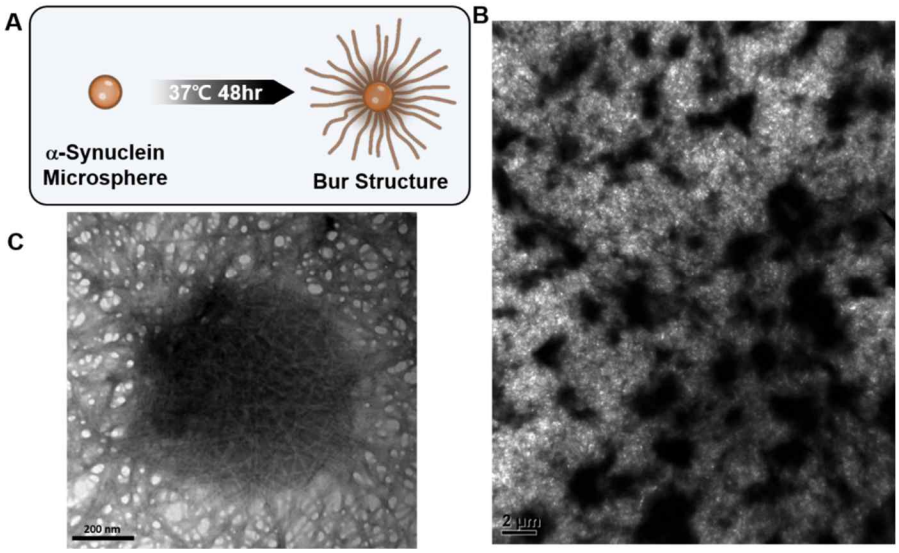


**Figure 44. Amyloid bur formation of αS microspheres.** (A) Schematic representation of amyloid bur formation from αS microsphere. (B) TEM image of amyloid bur structure in low magnification. (C) High magnification TEM image of amyloid bur structure.

Amyloid bur structures could be observed in all samples rather than in one spot on the TEM sample preparation (Figure 44C). Observing the Amyloid bur structure, the surface is densely packed with amyloid fibrils. This dense fibrils is a structure that could not be observed in the TEM data of the sample which was re-dissolved in water after freeze-drying. Therefore, it can be expected that adjusting these additional self-combining processes will increase their applicability.

## (5-2) Formation of amyloid bur structure with temperature

In order to check whether the αS microsphere structure can be selectively converted into amyloid bur structure, the experiment was carried out to incubate the produced microspheres by temperature. To equalize the amount of αS microspheres contained in each sample. Each αS microsphere prepared at a protein concentration of 1 mg / ml was dissolved in 1 ml of 20 mM pH 6.5 MES buffer, and the corresponding solutions were collected, gently mixed, and then again dispensed by 1 ml. As a result of observing the content of the β-sheet structure of the samples with thioflavin T binding assay, according to temperature showed that the microsphere structure showed no changed their

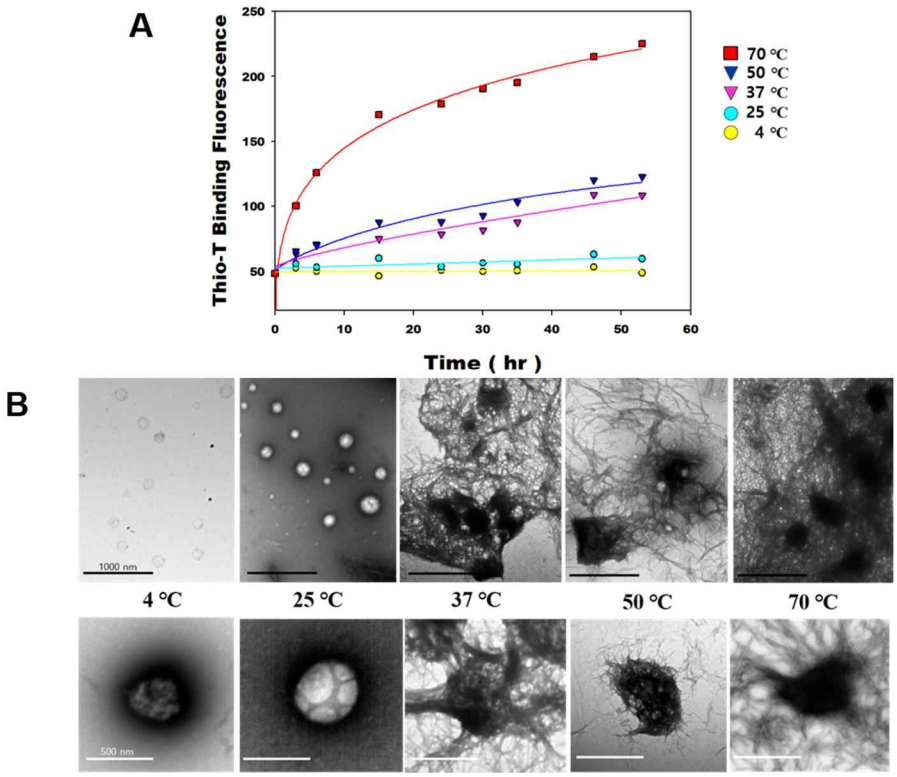


**Figure 45. Amyloid bur formation of αS microspheres under different temperatures.** (A) Thioflavin T binding fluorescence of αS microspheres incubated under different temperature. (B) TEM of each structures from microspheres was taken after end of incubation (54 h).

Thioflavin T binding value at 25 °C and 4 °C. Thioflavin T value was increased above 37 degrees, and it was observed that the tendency of the value increases rapidly with higher temperature (Figure 45A). The changes in the thioflavin T value obtained by incubating the microspheres was confirmed by observing the state of the microspheres with TEM after the incubation. At 4 °C and 25 °C the microspheres showed a stable state which did not change their morphologies after incubation. In the incubation at 37 °C or higher, amyloid but structure was formed, and longer fibril length was observed at higher temperature with TEM (Figure 45B).

## (5-3) Formation of amyloid bur in early stage

In order to confirm whether the amyloid bur structure derived from αS was derived from αS microspheres, the initial state of αS microspheres incubated at 70 °C was observed by TEM. When the incubation time was 1 h (Figure 46A), partial protein aggregates were observed on the surface of the αS microspheres. When the incubation time was 3 h (Figure 46B), it was observed that short fiber structures grew on the surface of the microspheres. When the incubation time was 5 h, much longer fibers grew on the surface of the αS microspheres (Figure 46C). Based on the results, it was confirmed that the

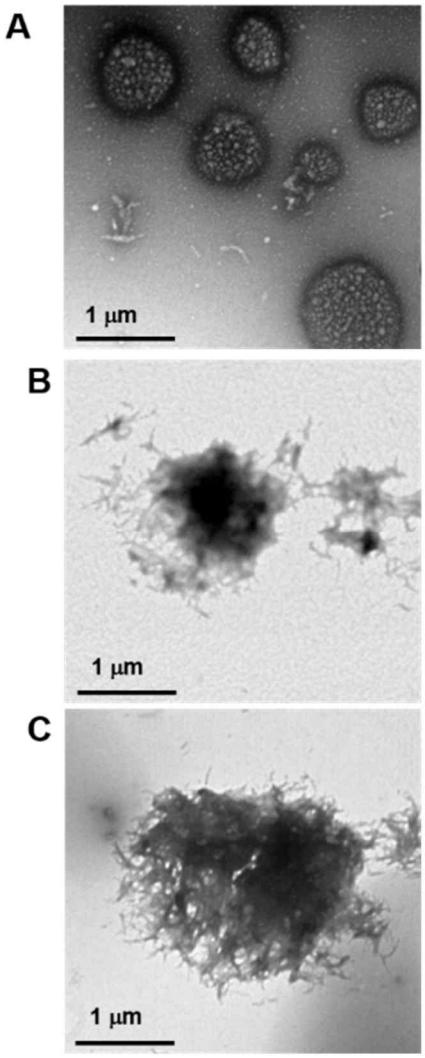


**Figure 46. TEM images of microspheres under incubation at 70 °C.** Amyloid bur formation from αS microspheres were observed with TEM (A) 1 h incubation, (B) 3 h incubation, (C) 5 h incubation of αS microspheres at 70 °C.

amyloid bur structure is not formed from other proteins or failed microspheres on the outside, but is formed in a form in which the length of the amyloid formed while maintaining the structure of the sphere is increased.

## (5-4) Toxicity of αS microspheres

In order to determine the toxicity of αS microspheres, experiments using Hela cells were performed. To provide an environment where the microspheres are completely converted to amyloid bur structure, after 48 hours of incubation at 37 °C, cell activity was compared. As a result, no toxic effects were observed for 48 hours at 37 °C (Figure 47). According to the reference, the spherical structure of proteins that form nanofibers through self-assembly is very toxic, such as amyloid-β or amylin.[80-81] Clear toxicity has been reported at concentrations of about one third and one quarter of the concentration tested in this study. However, the previously reported spherical structure is about 10 ~ 15 nm in size. Also, in these reports, as artificially increasing the size of the spherical structure, toxicity decreases, so two toxic requirements are reported: surface hydrophobicity and structure size. As results, αS microspheres in this study are outside the size of the range of toxicity.

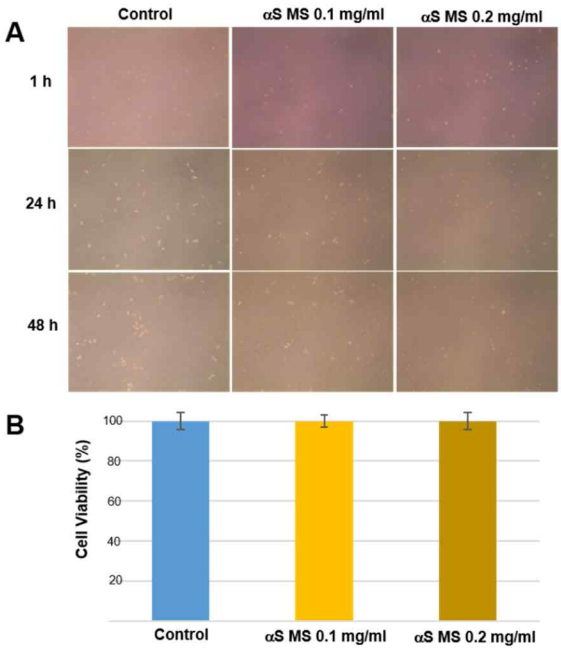


**Figure 47. Cell toxicity measurement with Hela cell.** (A) Optical microscopy image of HeLa cells with two αS Concentrations and incubation times. (B) Cell activity was observed by trypan blue assay

## (6) αS microspheres application as fill-in agent

Amyloid bur formation from microspheres was used as a fill-in agent in hydrogels for mechanical properties improvements (Figure 48A). Microspheres are placed on alginate hydrogel and heated to induce the additional assembly of microspheres to amyloid bur structure. The internal structure of the alginate hydrogel, the heat treated alginate hydrogel, and the amyloid bur structure induced alginate hydrogel experiment were confirmed by SEM. In the case of the alginate-only gel, there was no clear difference in the pore size of the hydrogel and the thickness of the network when the heat treatment was performed (Figure 48C) or not (Figure 48B). Surprisingly, inside the alginate gel, which induced the amyloid bur structure in the alginate hydrogel, a network with a thickness of between 20 and 50 nm was observed (Figure 48D). In order to observe the change in physical properties, the physical properties of the hydrogels were measured by a tensile test using universal testing machine (UTM). The final length of the alginate hydrogel was 10.17 mm, the fracture point was 176 kPa (Figure 49A). The final length of the alginate hydrogel, which experienced thermal stimulation, was 9.59 mm and the fracture point was 671 kPa (Figure 49B). It can be evaluated that partial internal network was improved, which is consistent with what has been reported previously.[82] On the other hand, hydrogels, which have αS microspheres placed inside the alginate

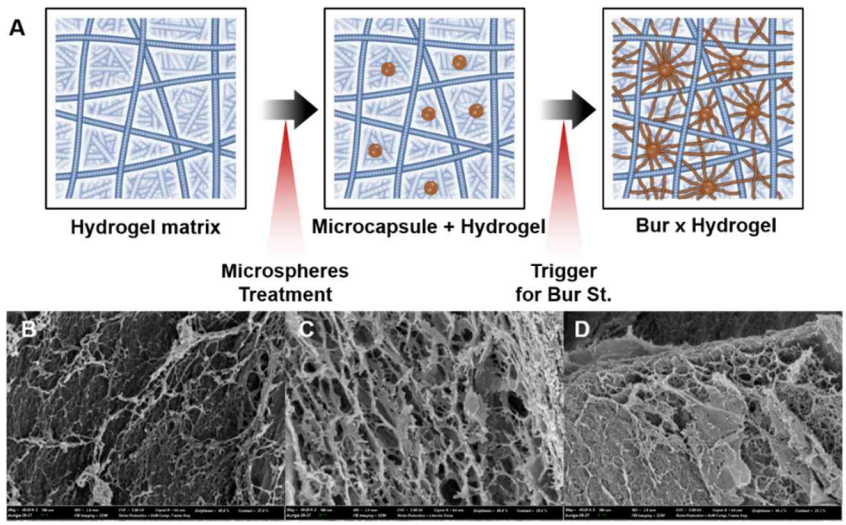


**Figure 48. Amyloid bur application with alginate hydrogel.** (A) Schematic representation of amyloid-bur structure in hydrogel scaffold. SEM image of (A) alginate hydrogel, (B) alginate hydrogel with heat treatment, and (C) alginate hydrogel with heat treated with αS microspheres.

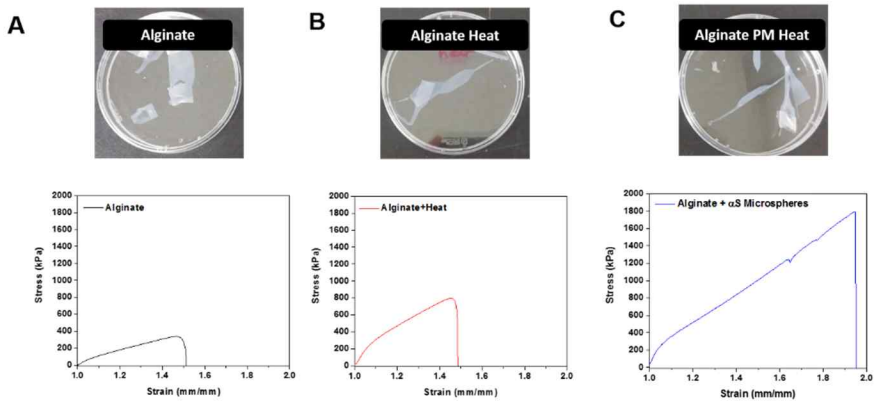


**Figure 49. Mechanical properties of αS microspheres embedded alginate hydrogel.** Optical images and stress-strain curves obtain with universal testing machine (UTM) of (A) alginate hydrogel, (B) alginate hydrogel with heat treatment, and (C) αS microspheres embedded alginate hydrogel after heat treatment.

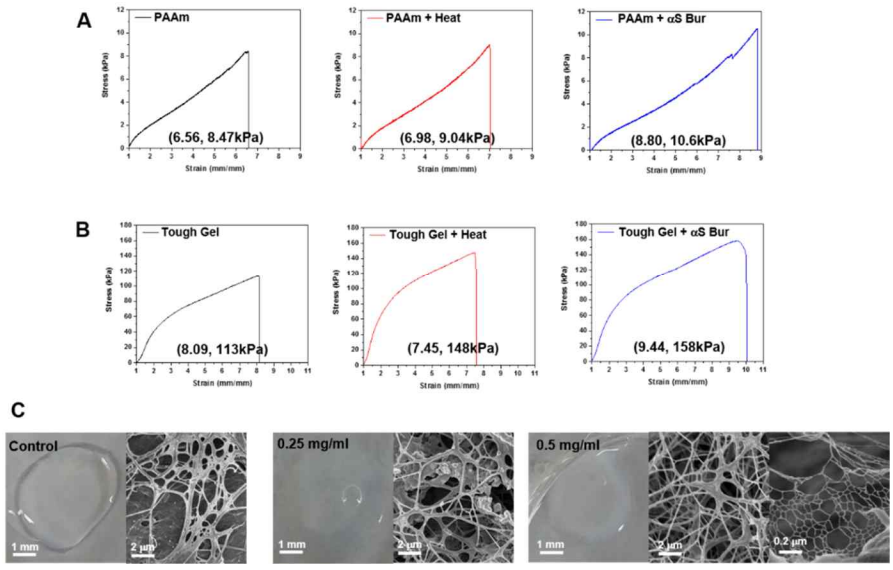


**Figure 50. Mechanical properties of αS microspheres embedded hydrogel.** Stress-strain curves obtain with universal testing machine (UTM) of (A) PAAm control hydrogel(left), after heat treatment(mid), and heat treated with αS microspheres(right). (B) Control of PAAm-alginate hydrogel (left), after heat treatment (middle), and heat treated with αS microspheres (right) tough hydrogel with heat treatment, and (C) Optical images and SEM images of collagen hydrogel (left) and αS microspheres embedded collagen hydrogel after heat treatment with different concentration of treated αS microspheres (right).

gel and induce amyloid bur structure through thermal stimulation, have a final length of 18.98 mm and a fracture point of 1794.82 kpa (Figure 49C). As result, the hydrogel properties were improved by inducing amyloid bur structure, which confirmed that αS microspheres can be used as an effective material to selectively increase the required physical properties as needed.

This feature of was not observed only in alginate hydrogels. In the hydrogel using polyacrylamide gel or tough hydrogel using polyacrylamide gel and alginate, the physical properties of the hydrogel were improved (Figure 50). And collagen gel was able to confirm the characteristics as such a fill in agent. The collagen gel used in the experiment was very soft, so the physical properties could not be measured, but the cloudy network was identified inside the naked eye (Figure 50C). Observation of the collagen gel through SEM revealed a nano scale of pore network that appears partially inside the collagen gel treated with high concentrations of αS microspheres (Figure 50C, right). These results indicate that the application of αS microspheres as fill in agent is applicable not only to alginate hydrogels and polyacrylamide hydrogels, but also to tough hydrogels with already improved physical properties and collagen hydrogels.

## (7) Additional applications of αS microspheres

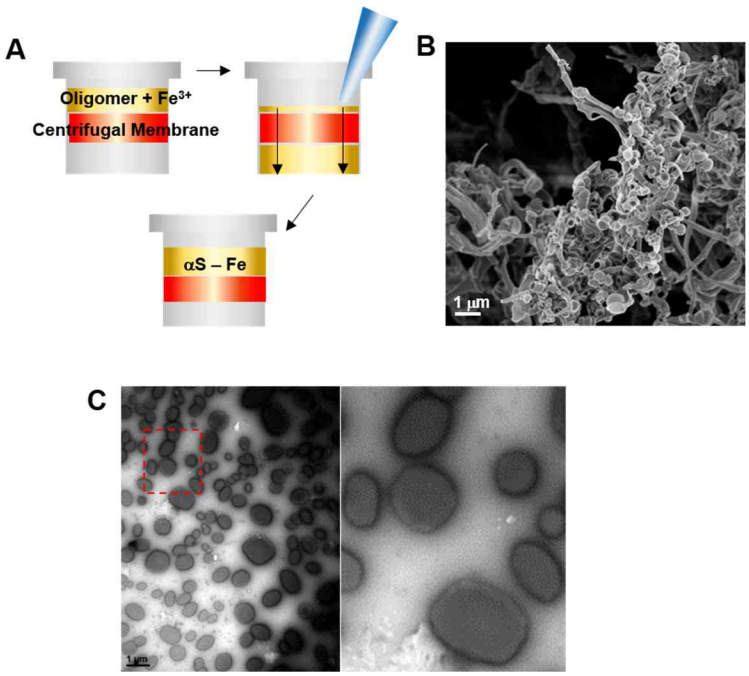


**Figure 51. αS microsphere formation with $Fe^{3+}$ ion.** (A) Scheme of preparation of αS oligomer-$Fe^{3+}$ conjugate. (B) SEM image of αS microspheres with $Fe^{3+}$ and (C) TEM image of resolved αS-$Fe^{3+}$ microspheres in DW.

The applicability of αS microspheres can be broadened by adding materials at the stage of preparation of microspheres or after preparation. αS microspheres were prepared by adding iron ions known to react with αS.[83] Formation of microspheres was confirmed with SEM and TEM (Figure 51), and the formed microspheres showed an external characteristic with more mass expression than the previously produced microspheres of αS. As a result, αS microspheres can be prepared by adding various substances known to bind with αS to produce spheres in which the materials coexist with αS.[84-86] Microspheres fabricated on this principle can be further extended if additional structural modifications to amyloid burs are considered. Under the condition that appropriate αS microspheres can be differentiated into amyloid burs, iron ion containing αS microspheres containing iron ions can also help to improve the various phenomena of iron deficiency in the body such as iron-deficiency anemia,[87-88] short breathing,[89] and headaches.[90] Additional structural modifications to amyloid burs were controlled only by temperature in this study. Although additional structural modifications to the amyloid burr were possible from the temperature control very selectively, when other additional change was adopted, such as physical stimulus, external environment, could not induce microsphere structural deformation in the scope of this study. One idea is to find clues from the various forms of mutants present in αS. Including not only the mutants studied directly for association with the disease such as A30P, E46K, H50Q, G51D, A53T,[91] but also include those known to be involved in the various self-

assembly of αS, such as .Y136C and A53C.[92-93] These mutants have different reactions to the external environment as well as the self-assembly of αS alone, which can be of interest if applied to these mutants.[94] Considering the size of the amyloid bur derived from the αS microspheres, it may also give an idea to explain the pathologically generated spherical fiber bundles in micro-scales. [95-97]

# II-3. Conclusions

Based on the contents of Part II, conclusion follows (Figure 52).

1. αS microspheres were prepared using αS oligomers.

2. αS microspheres were fabricated in three stages: rapid cooling, frozen annealing, freeze drying, and optimum experimental conditions were obtained through various experimental conditions for each step.

3. αS microspheres were stable when dissolved in water at room temperature, and this notable stability is due to the partial β-sheet structure generated during processing.

4. Amyloid bur structure was fabricated based on additional self-assembly of αS microsphere.

5. Formation of amyloid bur structure could be controlled by temperature and

showed excellent stability stable for more than 54 h at 4°C and 25°C.

6. The formation of amyloid bur structure could improve the mechanical properties of hydrogels.

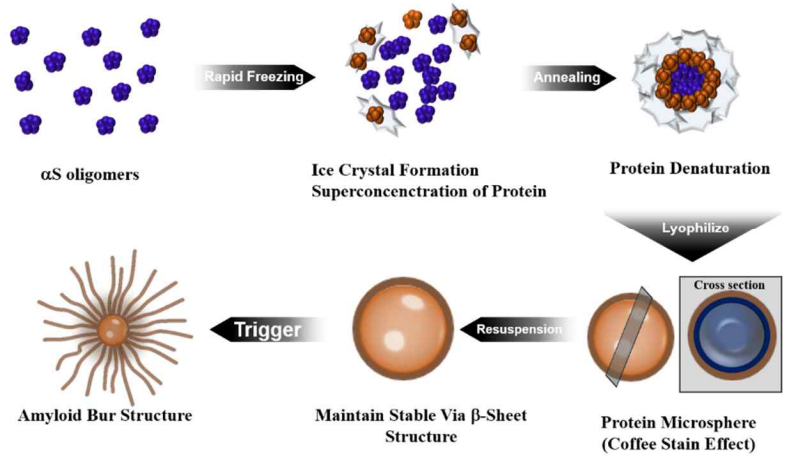


**Figure 52. Conclusion Part II.**

# Experimental section

## 1. Purification of αS

Human recombinant αS and αS Y136C mutant were separately overexpressed in *E. coli* and purified according to the procedures described in the previous reports.[92, 98] Human recombinant αS was cloned in pRK172 in *E. Coli* BL21. The *E. Coli* containing αS was cultured in LB agar plate. A single colony of cells transformed to 1 L of LB media containing 0.1 mg/ml ampicillin. After observing cell growth with UV at 600nm reaches 0.6 then the LB media was induced with 0.5 mM of IPTG (isopropylthiogalactoside) and incubated additional 4 h. The cells were harvested with centrifuge and the pellet was lysed with freezing-thawing method and 50mL per 1L culture media of lysis buffer (10 units/mL DNase, 0.1 mg/mL lysozyme, 2mM EDTA, 0.1 M NaCl, 0.1 mM PMSF 1 μg/mL leupeptin in 20 mM Tris – HCL pH 7.5 buffer). After lysis, only the supernatant was boiled at 100 °C for 20 min and cooled immediately with ice-water. The precipitate of solution was removed with centrifuge and additional syringe filtering (with pore size 0.22 μm). The lysate was purified with three chromatography columns. First DEAE sephacel for anion exchange, second S-200 for size exclusion, and finally with S-separose for cation exchange (Figure 53). After dialysis with 4L of MES (20mM, pH 6.5) buffer, the αS were stored at -80°C. αS Y136C mutant was purified with same procedure with brief modification to prohibit oxidation and dimerization

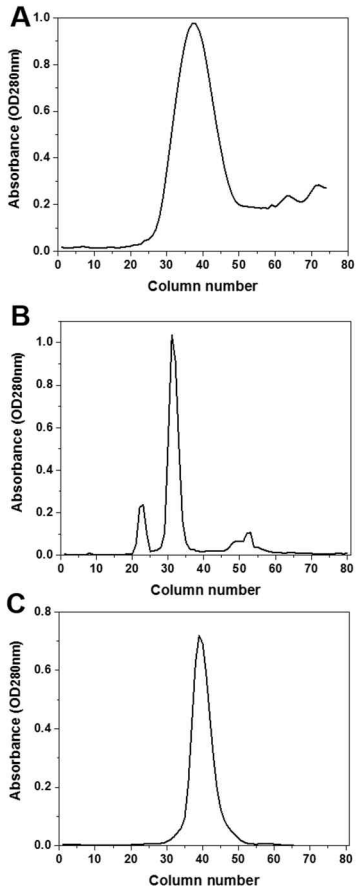


**Figure 53. Results of three columns in the purification of αS.** Columns were run to purify the αS and the optical density at 280 nm was measured after each column. (A) DEAE, (B) S-200, and (C) S-separose.

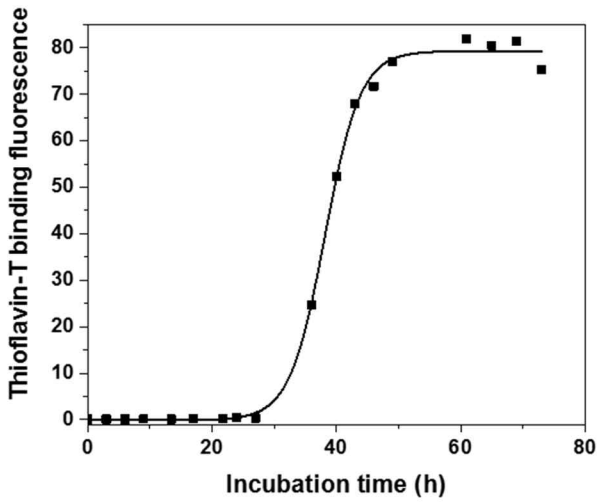


**Figure 54. Kinetics of αS self-assembly.** αS self-assembly process monitored with Thioflavin-T binding fluorescence.

of Y136C.

## 2. Thioflavin T binding assay

αS (1.0 mg/mL) in 20 mM MES buffer (pH 6.5) was incubated in 37 °C shaking incubator with rotation speed of 200 rpm. To observe amyloid fibril formation of αS, αS was mixed with 2.5 mM Thioflavin T in 50 mM glycin buffer (pH 8.5). The reaction of sample was induced in dark chamber for 5 min, and the fluorescence at 485 nm was monitored with excitation at 450 nm using luminescence spectrometer (LS-55B, Perkin-Elmer). Kinetics of αS shaking incubation confirmed the lag phase, exponential phase, and stationary phase, which were presented as sigmodal curves (Figure 54).

## 3. Preparation of αS film

αS film was produced with αS monomer at 1 mg/mL in 20 mM MES (pH 6.5) following a quiescent incubation at 50 ℃ for 48 h. The total volume of 1 mL was incubated in Eppendorf-tube (E-tube) at the temperature kept constant with ALB64 thermo bath (Fine PCR, Korea). To provide an oil-water interface, 300 μL of paraffin oil was carefully layered on top of the αS-containing aqueous solution without disturbing the interface. For the production of amyloid fibrils,

αS was subjected to either quiescent or agitated incubation at 200 rpm (Shaking Incubator VS8480S, Vision Scientific, Korea) at 37 ºC for various durations.

## 4. Preparation of αS Y136C-Alexa Flour 488 and its assembly into films and amyloid fibrils

αS Y136C mutant was labeled with Alexa Fluor 488 C5 maleimide by incubating them in 20 mM Tris-Cl (pH 7.5) for 12 h at 4 ºC. High performance liquid chromatography was used to remove the unreacted dye by employing C4 column. The αS-Alexa-488 conjugate was incubated in 20 mM MES (pH 6.5) at either 37 ºC or 50 ºC under agitated and quiescent condition, respectively. The resulting amyloid fibrils and films were examined with a confocal laser scanning microscope (LSM710, Carl Zeiss, Germany). Images were obtained using ZEN imaging software.

## 5. JC-1 and ANS binding assay

JC-1 (5,5 ,6,6 - tetrachloro-1,1,3,3 –tetraethylbenzimidazolyl carbocyanine iodide) binding intensity was measured according to previous report.[99] In brief, 1.5μm of JC-1 was mix with αS and the fluorescence spectrum between 500 and 600 nm with excitation at 490 nm was observed. In case of ANS (8-Anilino-1-naphthalenesulfonic acid), to monitor the bulk state of αS-Film solution, 50 μM of ANS was combined with 1mg/mL of αS.[24] After 5 min

reaction, the samples were estimated with emission range 400 and 600 nm with excitation at 350 nm using luminescence spectrometer (LS-55, Perkin Elmer).

## 6. Transmission electron microscopy

Aliquot of the sample containing αS (10 μL) was placed onto carbon-coated 200-mesh copper grid (Electron Microscopy Science, Hatfield, PA) and air-dried. After staining with 2 % uranyl acetate for 30 s, the specimen was examined with a transmission electron microscope of JEM1010 (JEOL, Tokyo, Japan).

## 7. Atomic force microscopy

To assess the protein film with AFM, an aliquot (100 μL) containing αS films was placed on $SiO_2$ wafer (PJ40227-6, Global wafers Co., Taiwan) which was previously cleaned with distilled water and purged with nitrogen gas before use. Following an adsorption for 2 h at room temperature, the wafer was washed with distilled water 5 times. The αS film on the wafer was analyzed with AFM (NX-10, Park System, Korea) in a non-contact mode. The obtained images were processed with XEI imaging software (Park System, Korea).

## 8. Optimal conditions for the αS film formation

To find pH optimum of the film formation, 20 mM citric acid - 20 mM sodium phosphate was prepared to make the solution with various pHs. αS was dialyzed overnight at 4 ºC against the citrate-phosphate at each pH with two changes for a total volume of 3 L. For the film formation in the presence of NaCl and sucrose, αS was incubated at 1 mg/ml in 20 mM MES (pH 6.5) containing either NaCl or sucrose at the concentrations tested.

## 9. Attenuated total reflectance-fourier transformation infrared spectrophotometer (ATR-FTIR)

The samples of αS monomers, αS films, αS fibrils, and αS microspheres were lyophilized using a freeze-dryer (EYELA FDU-2200, Tokyo Rikakikai, Japan), and analyzed with an FTIR spectrophotometer (Nicolet 6700, Thermo Scientific, WI). The FTIR spectra were obtained at a resolution of 4 $cm^{-1}$ using a triglycine sulfate (DTGS) KBr detector. The second derivative spectra obtained at amide I band region (1700 – 1600 $cm^{-1}$) were used to identify the frequencies of peaks for the subsequent curve fitting. Each deconvolved curve was fitted to a Gaussian curve using Origin Pro 2015 software (Origin Lab Corporation, Northampton, MA).

## 10. Circular dichroism spectroscopy (CD)

Protein secondary structures of αS monomers, films, and amyloid fibrils prepared in 20 mM MES at pH 6.5 to the final concentration of 0.33 mg/ml were assessed with CD spectroscopy (J-815, Jasco, Japan) scanned between 190 and 250 nm using 0.1-mm path length quartz cell. All the CD spectra were obtained as an average of three separate scans with a step resolution of 1.0 nm, a bandwidth of 1.0 nm, and a scan speed of 20 nm/min.

## 11. Preparation of cell attachment experiments

Cell adhesion experiments were conducted with Hela cells. Sufficient amount of Hela cells were incubated from stock and sub cultured to petri-dish. Equal amounts of cells were injected into the film treated and untreated glass and washed one hour later with culture media (DMEM). The number of attached cells was statistically generated from four photographs of three samples each, and an error bar was displayed.

## 12. Preparation of PCDA-αS film

The PCDA-αS hybrid film was prepared by incubating PCDA with the pre-formed αS film obtained from the oil-water interface at the final concentration of 1 mM.[48] The PCDA dissolved in 50 μL DMSO was combined with the αS

film and co-incubated for 2 h. The PCDA-αS hybrid film (0.5 mg/500 μl) was located on the surface of Whatman filter paper via suction with vacuum and then exposed to UV at 254 nm for 10 min to obtain a blue state. Its colorimetric transition to red was done as the film on the paper was heated to 80 ºC for 3 min.

## 13. Chemical and mechanical stability of the αS film and PCDA-αS hybrid film

Chemical stability of the αS film and PCDA-αS hybrid film (UV and heat treated) was evaluated with trypsin. Both films were subjected to the trypsin treatment at 0.1 mg/mL in 20 mM MES (pH 6.5) for 30 and 50 min at room temperature. The resulting films were examined with TEM. To test their mechanical stability, both αS film and PCDA-αS hybrid film were sonicated with a microtip-type ultrasonic processor (VCX 750, Sonics & Materials Inc., CT) at 20 kHz under 750 W with an on/off cycle of 10 s each. After 6 cycles of the sonication in ice, the final states of both films were examined with TEM.

## 14. Conductivity of the αS film and PCDA-αS hybrid film

Both αS film and PCDA-αS hybrid film were placed onto $SiO_2$ wafer (PJ40227-6, Global wafers Co., Taiwan) within 0.5 mL each. After 4 h of adsorption in a vacuum chamber, the wafers were washed with distilled water.

For the PCDA-αS hybrid film, in particular, it was subjected to the UV and heat treatments followed by drying under vacuum. With the completely dried films, silver paste (CANS, Japan) was applied to both sides of the wafer and dried in a vacuum chamber. The wafers were prepared 15 mm x 15 mm in size, and the length of applied silver paste was 5 mm on each side. Current (I)-voltage (V) measurements were carried out by using a potentiostat (Solartron 1480, Ametek, PA) at a scan rate of 50 mV/s.

## 15. Colorimetric responses of PCDA-αS Film structure

Colorimetric responses of PCDA-αS film structure to temperature, ethanol, pH was monitored by 100 μL of PCDA-αS film solution. For temperature, each samples were localized at the temperatures using ALB64 thermo bath (Fine PCR, Korea). For ethanol, each samples were diluted to according concentrations of ethanol while maintaining total volume of samples and amount of αS-film. To monitor the reactions in each pHs, centrifugation was done to remove 20mM MES buffer and 20 mM citric acid - 20 mM sodium phosphate buffer was used to resuspend PCDA-αS films.

## 16. Preparation of protein microspheres with αS

Protein microspheres were prepared with αS oligomers. αS oligomers were

prepped during the shaking incubation in 20 mM MES (pH 6.5) buffer.[70]

$$y = y_0 + \frac{a}{1 + e^{-(\frac{x - x_0}{b})}}$$

where $y$ is the measured fluorescence intensity; $y_0$ is the initial value of fluorescence; $a$ is the maximum intensity; $x_0$ is the time to reach 50% of $a$; $1/b$ is the apparent first-order rate constant ($k_{app}$) for the fibril growth. The time-point for collecting αS oligomers was determined at $x_0 - 4b$ when the fluorescence intensity is 1.8% of $a$. αS oligomers were separated form 20 mM MES buffer and dissolved to distilled water. Then the oligomers in distilled water was rapidly frozen using liquid nitrogen. The frozen aqueous solution was kept frozen over 5 h for frozen annealing. Then, microspheres were prepared by sufficient lyophilizing the frozen solution using freeze dryer (EYELA FDU-2200, Japan).

## 17. Scanning electron microscope (SEM)

Morphology of protein microsphere composed with αS was coated with sputter coater (EM ACE200, Leica). To monitor the details of the microspheres, the samples were completely dried and coated to 15nm thickness of Pt. Coated microspheres were observed with scanning electron microscope (AURIGA, Carl Zeiss / SUPRA 55VP, Carl Zeiss, Germany). Focused ion beam (FIB) was done with scanning electron microscope

(AURIGA, Carl Zeiss, Germany).

## 18. Preparation of αS-eosin microspheres

To monitor the morphology of αS microspheres, Eosin Y and αS oligomers were co-incubated for 1 h in room temperature and formed microspheres using procedure mentioned above.

## 19. αS protein microspheres stability

Lyophilized protein microspheres were dissolved again in distilled water. In order to secure the stability of the spherical structure, the melting process was performed by gently shaking the 1 ml Eppendorf-tube. In order to observe stability in distilled water, samples were observed at intervals of 15 minutes immediately after dissolving in distilled water by TEM.

## 20. Measurement of αS microsphere size according to αS concentration

Incubated αS oligomers were divided by concentration into E-tubes. In this experiment, rapid cooling stimulation was performed immediately to prevent the degradation of the oligomer when the low concentration was reached.

Afterwards, αS microspheres were manufactured through three stages of rapid cooling, frozen annealing and freeze drying. The size of the microspheres per sample was evaluated by measuring the size of all microspheres appearing in five SEM images per sample.

## 21. Preparation of amyloid bur structure from αS microspheres

Production experiments of amyloid burs were observed according to temperature difference. Five individual cultured samples were incubated to form oligomers and followed procedures of rapid cooling (freezing) – annealing – freeze drying. Freeze dried microspheres were collected in one place and then divided into five so that the concentrations of microspheres were the same for each sample. In order to reduce the stimulation to spherical structure, 20mM MES buffer was used in the amyloid bur structure forming under different temperature experiment.

## 22. Measurement of αS microsphere toxicity

Experiments were carried out incubation of αS microspheres in HeLa cells. The final time was set to 48 hr to confirm that the αS microspheres were completely converted to amyloid bur. Hela cells were incubated with DMEM medium and incubated with 10% fatal bovine serum. After incubation, the

cells were detached from the plate using trypsin and applied tyrpan blue assay on these cells.

## 23. Preparation of hydrogels

To prepare alginate hydrogel, 2% Sodium alginate was dissolved in water. To completely dissolve in the solution, the temperature of the water was raised to 50 °C and then stirred with a plastic stick until it was completely dissolved.[100] The solution was placed in a glass cast with spacer thickness of 2 mm. And the solution in spacer was put in to 0.3 M $CaCl_2$ to induce ionic crosslinking between alginate chains for 10 h. The hydrogel was cut to 'dog-bone' shape to test mechanical properties with universal testing machine. To prepare acrylamide hydrogel 13.6% acrylamide was dissolved in water. Using same spacer mentioned above, 0.03mol% of MBA (*N*,*N*′-Methylenebis (acrylamide) was used with ammonium persulfate and temed. In case of tough gel, 12.5% of acrylamide and 0.5% alginate was used with separated cross linking.[101]

## 24. Preparation of amyloid bur in hydrogels

To fabricated alginate – amyloid bur hydrogel, microsphere embedded hydro gel was prepared. Microspheres were located in water after hydrogel monomers were completely dissolved. To prevent the microspheres from

breaking in the insoluble state, the mixture was slowly stirred with a plastic rod until the microspheres dissolved in solution. Thereafter, the sample was vigorously stirred using a vortexer to ensure the uniformity of the sample in the sample. After sufficient crosslinking, the alginate – microspheres hydrogel was treated with heat of 70 °C for overnight and 37 °C for acrylamide gel and tough gel. Considering the evaporation that takes place in the sample, the sample incubation was proceeded with the flask completely sealed with a sufficient amount of distilled water inside.

## 25. Universal testing machine (UTM)

Universal testing machine (UTM, AGS-X50N, Shimadzu, Japan) was used to test mechanical properties of hydrogel. The strength of the forceps to which the sample was collected had to be adjusted to prevent the sample from breaking. Velocity of tensile test was 50mm/min.

# References


1. Beyer, K., Mechanistic aspects of Parkinson's disease: alpha-synuclein and the biomembrane. *Cell Biochem Biophys* **2007,** *47* (2), 285-299.

2. Dev, K. K.; Hofele, K.; Barbieri, S.; Buchman, V. L.; van der Putten, H., Part II: alpha-synuclein and its molecular pathophysiological role in neurodegenerative disease. *Neuropharmacology* **2003,** *45* (1), 14-44.

3. Moore, D. J.; West, A. B.; Dawson, V. L.; Dawson, T. M., Molecular pathophysiology of Parkinson's disease. *Annu Rev Neurosci* **2005,** *28*, 57-87.

4. Harper, J. D.; Wong, S. S.; Lieber, C. M.; Lansbury, P. T., Observation of metastable Abeta amyloid protofibrils by atomic force microscopy. *Chem Biol* **1997,** *4* (2), 119-25.

5. Walsh, D. M.; Lomakin, A.; Benedek, G. B.; Condron, M. M.; Teplow, D. B., Amyloid beta-protein fibrillogenesis. Detection of a protofibrillar intermediate. *J Biol Chem* **1997,** *272* (35), 22364-72.

6. Scherzinger, E.; Sittler, A.; Schweiger, K.; Heiser, V.; Lurz, R.; Hasenbank, R.; Bates, G. P.; Lehrach, H.; Wanker, E. E., Self-assembly of polyglutamine-containing huntingtin fragments into amyloid-like fibrils: implications for Huntington's disease pathology. *Proc Natl Acad Sci U S A* **1999,** *96* (8), 4604-9.

7. Anguiano, M.; Nowak, R. J.; Lansbury, P. T., Jr., Protofibrillar islet amyloid polypeptide permeabilizes synthetic vesicles by a pore-like mechanism that may be relevant to type II diabetes. *Biochemistry* **2002,** *41* (38), 11338-43.

8. Chiti, F.; Dobson, C. M., Protein misfolding, functional amyloid, and human disease. *Annu. Rev. Biochem.* **2006,** *75*, 333-66.

9. Adamcik, J.; Jung, J. M.; Flakowski, J.; De Los Rios, P.; Dietler, G.; Mezzenga, R., Understanding amyloid aggregation by statistical analysis of atomic force microscopy images. *Nat Nanotechnol* **2010,** *5* (6), 423-428.

10. Selkoe, D. J., Folding proteins in fatal ways. *Nature* **2003,** *426* (6968), 900-904.

11. Dirix, C.; Meersman, F.; MacPhee, C. E.; Dobson, C. M.; Heremans, K., High hydrostatic pressure dissociates early aggregates of TTR105-115, but not the mature amyloid fibrils. *J Mol Biol* **2005,** *347* (5), 903-9.

12. Smith, J. F.; Knowles, T. P.; Dobson, C. M.; Macphee, C. E.; Welland, M. E., Characterization of the nanoscale properties of individual amyloid fibrils. *Proc Natl Acad Sci U S A* **2006,** *103* (43), 15806-11.

13. Petkova, A. T.; Leapman, R. D.; Guo, Z.; Yau, W. M.; Mattson, M. P.; Tycko, R., Self-propagating, molecular-level polymorphism in Alzheimer's beta-amyloid fibrils. *Science* **2005,** *307* (5707), 262-5.

14. Dai, B.; Li, D.; Xi, W.; Luo, F.; Zhang, X.; Zou, M.; Cao, M.; Hu, J.; Wang, W.; Wei, G.; Zhang, Y.; Liu, C., Tunable assembly of amyloid-forming peptides into nanosheets as a retrovirus carrier. *Proc Natl Acad Sci U S A* **2015,** *112* (10), 2996-3001.

15. Bhak, G.; Lee, S.; Park, J. W.; Cho, S.; Paik, S. R., Amyloid hydrogel derived from curly protein fibrils of alpha-synuclein. *Biomaterials* **2010,** *31*

(23), 5986-95.

16. Peralta, M. D.; Karsai, A.; Ngo, A.; Sierra, C.; Fong, K. T.; Hayre, N. R.; Mirzaee, N.; Ravikumar, K. M.; Kluber, A. J.; Chen, X.; Liu, G. Y.; Toney, M. D.; Singh, R. R.; Cox, D. L., Engineering amyloid fibrils from beta-solenoid proteins for biomaterials applications. *ACS Nano* **2015,** *9* (1), 449-63.

17. Sipe, J. D., Amyloidosis. *Annu. Rev. Biochem.* **1992,** *61*, 947-75.

18. Eliezer, D., Biophysical characterization of intrinsically disordered proteins. *Curr Opin Struct Biol* **2009,** *19* (1), 23-30.

19. Maiti, N. C.; Apetri, M. M.; Zagorski, M. G.; Carey, P. R.; Anderson, V. E., Raman spectroscopic characterization of secondary structure in natively unfolded proteins: alpha-synuclein. *J Am Chem Soc* **2004,** *126* (8), 2399-408.

20. Bartels, T.; Ahlstrom, L. S.; Leftin, A.; Kamp, F.; Haass, C.; Brown, M. F.; Beyer, K., The N-terminus of the intrinsically disordered protein alpha-synuclein triggers membrane binding and helix folding. *Biophys J* **2010,** *99* (7), 2116-24.

21. Jao, C. C.; Hegde, B. G.; Chen, J.; Haworth, I. S.; Langen, R., Structure of membrane-bound alpha-synuclein from site-directed spin labeling and computational refinement. *P Natl Acad Sci USA* **2008,** *105* (50), 19666-19671.

22. Lee, J. H.; Hong, C. S.; Lee, S.; Yang, J. E.; Park, Y. I.; Lee, D.; Hyeon, T.; Jung, S.; Paik, S. R., Radiating amyloid fibril formation on the surface of lipid membranes through unit-assembly of oligomeric species of alpha-

synuclein. *PLoS One* **2012,** *7* (10), e47580.

23. Naiki, H.; Gejyo, F., Kinetic analysis of amyloid fibril formation. *Methods Enzymol.* **1999,** *309*, 305-18.

24. Bhak, G.; Lee, J.; Kim, T. H.; Lee, S.; Lee, D.; Paik, S. R., Molecular inscription of environmental information into protein suprastructures: temperature effects on unit assembly of alpha-synuclein oligomers into polymorphic amyloid fibrils. *Biochem. J.* **2014,** *464* (2), 259-69.

25. Lee, C. H.; Singla, A.; Lee, Y., Biomedical applications of collagen. *Int J Pharm* **2001,** *221* (1-2), 1-22.

26. Skarja, G. A.; Brash, J. L.; Bishop, P.; Woodhouse, K. A., Protein and platelet interactions with thermally denatured fibrinogen and cross-linked fibrin coated surfaces. *Biomaterials* **1998,** *19* (23), 2129-2138.

27. Um, I. C.; Kweon, H. Y.; Park, Y. H.; Hudson, S., Structural characteristics and properties of the regenerated silk fibroin prepared from formic acid. *Int J Biol Macromol* **2001,** *29* (2), 91-97.

28. Yamauchi, K.; Yamauchi, A.; Kusunoki, T.; Kohda, A.; Konishi, Y., Preparation of stable aqueous solution of keratins, and physiochemical and biodegradational properties of films. *J Biomed Mater Res* **1996,** *31* (4), 439-444.

29. Prime, K. L.; Whitesides, G. M., Self-assembled organic monolayers: model systems for studying adsorption of proteins at surfaces. *Science* **1991,** *252* (5009), 1164-7.

30. Tharanathan, R. N., Biodegradable films and composite coatings: past, present and future. *Trends Food Sci Tech* **2003,** *14* (3), 71-78.

31. Lee, H.; Dellatore, S. M.; Miller, W. M.; Messersmith, P. B., Mussel-inspired surface chemistry for multifunctional coatings. *Science* **2007,** *318* (5849), 426-430.

32. Bunker, B. C.; Rieke, P. C.; Tarasevich, B. J.; Campbell, A. A.; Fryxell, G. E.; Graff, G. L.; Song, L.; Liu, J.; Virden, J. W.; Mcvay, G. L., Ceramic Thin-Film Formation on Functionalized Interfaces through Biomimetic Processing. *Science* **1994,** *264* (5155), 48-55.

33. Buchko, C. J.; Chen, L. C.; Shen, Y.; Martin, D. C., Processing and microstructural characterization of porous biocompatible protein polymer thin films. *Polymer* **1999,** *40* (26), 7397-7407.

34. Marjo, C. E.; Gatenby, S.; Rich, A. M.; Gong, B.; Chee, S., ATR-FTIR as a tool for assessing potential for chemical ageing in Spandex/Lycra (R)/elastane-based fabric collections. *Stud Conserv* **2017,** *62* (6), 343-353.

35. Lu, J. T.; Lee, C. J.; Bent, S. F.; Fishman, H. A.; Sabelman, E. E., Thin collagen film scaffolds for retinal epithelial cell culture. *Biomaterials* **2007,** *28* (8), 1486-1494.

36. Oussalah, M.; Caillet, S.; Salmieri, S.; Saucier, L.; Lacroix, M., Antimicrobial and antioxidant effects of milk protein-based film containing essential oils for the preservation of whole beef muscle. *J Agr Food Chem* **2004,** *52* (18), 5598-5605.

37. Xu, H. T.; Ma, L.; Shi, H. F.; Gao, C. Y.; Han, C. M., Chitosan-hyaluronic acid hybrid film as a novel wound dressing: in vitro and in vivo studies. *Polym Advan Technol* **2007,** *18* (11), 869-875.

38. Lee, H.; Rho, J.; Messersmith, P. B., Facile Conjugation of Biomolecules onto Surfaces via Mussel Adhesive Protein Inspired Coatings. *Adv Mater* **2009,** *21* (4), 431-+.

39. Shu, X. Z.; Zhu, K. J.; Song, W. H., Novel pH-sensitive citrate cross-linked chitosan film for drug controlled release. *Int J Pharm* **2001,** *212* (1), 19-28.

40. Sriyudthsak, M.; Yamagishi, H.; Moriizumi, T., Enzyme-Immobilized Langmuir-Blodgett Film for a Biosensor. *Thin Solid Films* **1988,** *160* (1-2), 463-469.

41. Yang, C. K.; Dan, N. H.; You, W. T.; Huang, Y. P.; Chen, Y. N.; Yu, G. F.; Dan, W. H.; Wen, H. T., Modification of collagen-chitosan membrane by oxidation sodium alginate and in vivo/in vitro evaluation for wound dressing application. *Int J Polym Anal Ch* **2019,** *24* (7), 619-629.

42. Wantyghem, J.; Baron, M. H.; Picquart, M.; Lavialle, F., Conformational changes of Robinia pseudoacacia lectin related to modifications of the environment: FTIR investigation. *Biochemistry* **1990,** *29* (28), 6600-9.

43. Ariesandi, W.; Chang, C. F.; Chen, T. E.; Chen, Y. R., Temperature-dependent structural changes of Parkinson's alpha-synuclein reveal the role of

pre-existing oligomers in alpha-synuclein fibrillization. *PLoS One* **2013,** *8* (1), e53487.

44. Lee, J. C.; Timasheff, S. N., The Stabilization of Proteins by Sucrose. *Journal of Biological Chemistry* **1981,** *256* (14), 7193-7201.

45. Galmarini, M. V.; Baeza, R.; Sanchez, V.; Zamora, M. C.; Chirife, J., Comparison of the viscosity of trehalose and sucrose solutions at various temperatures: Effect of guar gum addition. *Lwt-Food Sci Technol* **2011,** *44* (1), 186-190.

46. Ainavarapu, R. K.; Brujic, J.; Huang, H. H.; Wiita, A. P.; Lu, H.; Li, L. W.; Walther, K. A.; Carrion-Vazquez, M.; Li, H. B.; Fernandez, J. M., Contour length and refolding rate of a small protein controlled by engineered disulfide bonds. *Biophysical Journal* **2007,** *92* (1), 225-233.

47. Lee, J.; Bhak, G.; Lee, J. H.; Park, W.; Lee, M.; Lee, D.; Jeon, N. L.; Jeong, D. H.; Char, K.; Paik, S. R., Free-standing gold-nanoparticle monolayer film fabricated by protein self-assembly of alpha-synuclein. *Angew Chem Int Ed Engl* **2015,** *54* (15), 4571-6.

48. Yang, J. E.; Park, J. S.; Cho, E.; Jung, S.; Paik, S. R., Robust Polydiacetylene-Based Colorimetric Sensing Material Developed with Amyloid Fibrils of alpha-Synuclein. *Langmuir* **2015,** *31* (5), 1802-1810.

49. Yang, J. E.; Lee, S.; Bhak, G.; Lee, M.; Jeong, D. H.; Jung, S.; Paik, S. R., Litmus-type thermochromic and solvatochromic sensors prepared with alpha-synuclein amyloid fibrils and polydiacetylene. *Sensor Actuat B-Chem*

**2016,** *227*, 313-319.

50. Okawa, Y.; Aono, M., Nanoscale control of chain polymerization. *Nature* **2001,** *409* (6821), 683-4.

51. Sun, A.; Lauher, J. W.; Goroff, N. S., Preparation of poly(diiododiacetylene), an ordered conjugated polymer of carbon and iodine. *Science* **2006,** *312* (5776), 1030-4.

52. Carpick, R. W.; Sasaki, D. Y.; Burns, A. R., First observation of mechanochromism at the nanometer scale. *Langmuir* **2000,** *16* (3), 1270-1278.

53. Peng, H. S.; Tang, J.; Yang, L.; Pang, J. B.; Ashbaugh, H. S.; Brinker, C. J.; Yang, Z. Z.; Lu, Y. F., Responsive periodic mesoporous polydiacetylene/silica nanocomposites. *Journal of the American Chemical Society* **2006,** *128* (16), 5304-5305.

54. Charoenthai, N.; Pattanatornchai, T.; Wacharasindhu, S.; Sukwattanasinitt, M.; Traiphol, R., Roles of head group architecture and side chain length on colorimetric response of polydiacetylene vesicles to temperature, ethanol and pH. *J Colloid Interf Sci* **2011,** *360* (2), 565-573.

55. Lee, H. Y.; Tiwari, K. R.; Raghavan, S. R., Biopolymer capsules bearing polydiacetylenic vesicles as colorimetric sensors of pH and temperature. *Soft Matter* **2011,** *7* (7), 3273-3276.

56. De Oliveira, T. V.; Soares, N. D. F.; Silva, D. J.; de Andrade, N. J.; Medeiros, E. A. A.; Badaro, A. T., Development of PDA/Phospholipids/Lysine vesicles to detect pathogenic bacteria. *Sensor Actuat B-Chem* **2013,** *188*, 385-

392.

57. Seo, S.; Lee, J.; Choi, E. J.; Kim, E. J.; Song, J. Y.; Kim, J., Polydiacetylene Liposome Microarray Toward Influenza A Virus Detection: Effect of Target Size on Turn-On Signaling. *Macromol Rapid Comm* **2013,** *34* (9), 743-748.

58. Kim, K. W.; Choi, H.; Lee, G. S.; Ahn, D. J.; Oh, M. K.; Kim, J. M., Micro-patterned polydiacetylene vesicle chips for detecting protein-protein interactions. *Macromol Res* **2006,** *14* (4), 483-485.

59. Kim, J. M.; Lee, Y. B.; Chae, S. K.; Ahn, D. J., Patterned color and fluorescent images with polydiacetylene supramolecules embedded in poly(vinyl alcohol) films. *Adv Funct Mater* **2006,** *16* (16), 2103-2109.

60. Du Plessis, J.; Ramachandran, C.; Weiner, N.; Muller, D. G., The influence of lipid composition and lamellarity of liposomes on the physical stability of liposomes upon storage. *Int J Pharm* **1996,** *127* (2), 273-278.

61. Carpick, R. W.; Sasaki, D. Y.; Marcus, M. S.; Eriksson, M. A.; Burns, A. R., Polydiacetylene films: a review of recent investigations into chromogenic transitions and nanomechanical properties. *J Phys-Condens Mat* **2004,** *16* (23), R679-R697.

62. Takami, K.; Mizuno, J.; Akai-Kasaya, M.; Saito, A.; Aono, M.; Kuwahara, Y., Conductivity measurement of polydiacetylene thin films by double-tip scanning tunneling microscopy. *J Phys Chem B* **2004,** *108* (42), 16353-16356.

63. Maerten, C.; Jierry, L.; Schaaf, P.; Boulmedais, F., Review of Electrochemically Triggered Macromolecular Film Buildup Processes and Their Biomedical Applications. *Acs Applied Materials & Interfaces* **2017,** *9* (34), 28117-28138.

64. Qi, H.; Zhang, C.; Guo, H.; Zheng, W.; Yang, J.; Zhou, X.; Zhang, L., Bioinspired Multifunctional Protein Coating for Antifogging, Self-Cleaning, and Antimicrobial Properties. *ACS Appl Mater Interfaces* **2019,** *11* (27), 24504-24511.

65. Han, U.; Kim, Y. J.; Kim, W.; Park, J. H.; Hong, J., Construction of nano-scale cellular environments by coating a multilayer nanofilm on the surface of human induced pluripotent stem cells. *Nanoscale* **2019,** *11* (28), 13541-13551.

66. Serio, T. R.; Cashikar, A. G.; Kowal, A. S.; Sawicki, G. J.; Moslehi, J. J.; Serpell, L.; Arnsdorf, M. F.; Lindquist, S. L., Nucleated conformational conversion and the replication of conformational information by a prion determinant. *Science* **2000,** *289* (5483), 1317-21.

67. Lee, J.; Culyba, E. K.; Powers, E. T.; Kelly, J. W., Amyloid-beta forms fibrils by nucleated conformational conversion of oligomers. *Nat. Chem. Biol.* **2011,** *7* (9), 602-9.

68. Fandrich, M., Oligomeric intermediates in amyloid formation: structure determination and mechanisms of toxicity. *J. Mol. Biol.* **2012,** *421* (4-5), 427-40.

69. Bhak, G.; Choe, Y. J.; Paik, S. R., Mechanism of amyloidogenesis: nucleation-dependent fibrillation versus double-concerted fibrillation. *BMB Rep.* **2009,** *42* (9), 541-51.

70. Bhak, G.; Lee, S.; Kim, T. H.; Lee, J. H.; Yang, J. E.; Joo, K.; Lee, J.; Char, K.; Paik, S. R., Morphological Evaluation of Meta-stable Oligomers of alpha-Synuclein with Small-Angle Neutron Scattering. *Sci Rep* **2018,** *8* (1), 14295.

71. Peyratout, C. S.; Dahne, L., Tailor-made polyelectrolyte microcapsules: From multilayers to smart containers. *Angew Chem Int Edit* **2004,** *43* (29), 3762-3783.

72. Slotta, U. K.; Rammensee, S.; Gorb, S.; Scheibel, T., An engineered spider silk protein forms microspheres. *Angew Chem Int Ed Engl* **2008,** *47* (24), 4592-4.

73. Daamen, W. F.; Geutjes, P. J.; van Moerkerk, H. T. B.; Nillesen, S. T. M.; Wismans, R. G.; Hafmans, T.; van den Heuvel, L. P. W. J.; Pistorius, A. M. A.; Veerkamp, J. H.; van Hest, J. C. M.; van Kuppevelt, T. H., "Lyophilisomes": A new type of (bio)capsule. *Adv Mater* **2007,** *19* (5), 673-+.

74. Cao, Z. B.; Chen, X.; Yao, J. R.; Huang, L.; Shao, Z. Z., The preparation of regenerated silk fibroin microspheres. *Soft Matter* **2007,** *3* (7), 910-915.

75. de Vries, A.; Gomez, Y. L.; Jansen, B.; van der Linden, E.; Scholten, E., Controlling Agglomeration of Protein Aggregates for Structure Formation

in Liquid Oil: A Sticky Business. *Acs Applied Materials & Interfaces* **2017,** *9* (11), 10136-10147.

76. Sanchez, M. A.; Kling, T.; Ishiyama, T.; van Zadel, M. J.; Bisson, P. J.; Mezger, M.; Jochum, M. N.; Cyran, J. D.; Smit, W. J.; Bakker, H. J.; Shultz, M. J.; Morita, A.; Donadio, D.; Nagata, Y.; Bonn, M.; Backus, E. H. G., Experimental and theoretical evidence for bilayer-by-bilayer surface melting of crystalline ice. *P Natl Acad Sci USA* **2017,** *114* (2), 227-232.

77. Wei, X.; Miranda, P. B.; Zhang, C.; Shen, Y. R., Sum-frequency spectroscopic studies of ice interfaces. *Phys Rev B* **2002,** *66* (8).

78. Jansson, H.; Swenson, J., The protein glass transition as measured by dielectric spectroscopy and differential scanning calorimetry. *Bba-Proteins Proteom* **2010,** *1804* (1), 20-26.

79. Roy, I.; Gupta, M. N., Freeze-drying of proteins: some emerging concerns. *Biotechnol Appl Bioc* **2004,** *39*, 165-177.

80. Hoshi, M.; Sato, M.; Matsumoto, S.; Noguchi, A.; Yasutake, K.; Yoshida, N.; Sato, K., Spherical aggregates of beta-amyloid (amylospheroid) show high neurotoxicity and activate tau protein kinase I/glycogen synthase kinase-3beta. *Proc Natl Acad Sci U S A* **2003,** *100* (11), 6370-5.

81. Green, J. D.; Goldsbury, C.; Kistler, J.; Cooper, G. J.; Aebi, U., Human amylin oligomer growth and fibril elongation define two distinct phases in amyloid formation. *J Biol Chem* **2004,** *279* (13), 12206-12.

82. Soazo, M.; Baez, G.; Barboza, A.; Busti, P. A.; Rubiolo, A.; Verdini,

R.; Delorenzi, N. J., Heat treatment of calcium alginate films obtained by ultrasonic atomizing: Physicochemical characterization. *Food Hydrocolloid* **2015,** *51*, 193-199.

83. Binolfi, A.; Rasia, R. M.; Bertoncini, C. W.; Ceolin, M.; Zweckstetter, M.; Griesinger, C.; Jovin, T. M.; Fernandez, C. O., Interaction of alpha-synuclein with divalent metal ions reveals key differences: A link between structure, binding specificity and fibrillation enhancement. *Journal of the American Chemical Society* **2006,** *128* (30), 9893-9901.

84. Peng, Y.; Wang, C. S.; Xu, H. H.; Liu, Y. N.; Zhou, F. M., Binding of alpha-synuclein with Fe(III) and with Fe(II) and biological implications of the resultant complexes. *J Inorg Biochem* **2010,** *104* (4), 365-370.

85. Binolfi, A.; Lamberto, G. R.; Duran, R.; Quintanar, L.; Bertoncini, C. W.; Souza, J. M.; Cervenansky, C.; Zweckstetter, M.; Griesinger, C.; Fernandez, C. O., Site-specific interactions of Cu(II) with alpha and beta-synuclein: Bridging the molecular gap between metal binding and aggregation. *Journal of the American Chemical Society* **2008,** *130* (35), 11801-11812.

86. Yang, J. E.; Rhoo, K. Y.; Lee, S.; Lee, J. T.; Park, J. H.; Bhak, G.; Paik, S. R., EGCG-mediated Protection of the Membrane Disruption and Cytotoxicity Caused by the 'Active Oligomer' of alpha-Synuclein. *Sci. Rep.* **2017,** *7* (1), 17945.

87. Camaschella, C., Iron-Deficiency Anemia. *New Engl J Med* **2015,** *372* (19), 1832-1843.

88. Matteson, K. A.; Raker, C. A.; Pinto, S. B.; Scott, D. M.; Frishman, G. N., Women Presenting to an Emergency Facility with Abnormal Uterine Bleeding Patient Characteristics and Prevalence of Anemia. *J Reprod Med* **2012,** *57* (1-2), 17-25.

89. Abbaspour, N.; Hurrell, R.; Kelishadi, R., Review on iron and its importance for human health. *J Res Med Sci* **2014,** *19* (2), 164-174.

90. Markey, K. A.; Mollan, S. P.; Jensen, R. H.; Sinclair, A. J., Understanding idiopathic intracranial hypertension: mechanisms, management, and future directions. *Lancet Neurol* **2016,** *15* (1), 78-91.

91. Flagmeier, P.; Meisl, G.; Vendruscolo, M.; Knowles, T. P. J.; Dobson, C. M.; Buell, A. K.; Galvagnion, C., Mutations associated with familial Parkinson's disease alter the initiation and amplification steps of alpha-synuclein aggregation. *P Natl Acad Sci USA* **2016,** *113* (37), 10328-10333.

92. Lee, D.; Choe, Y. J.; Choi, Y. S.; Bhak, G.; Lee, J.; Paik, S. R., Photoconductivity of pea-pod-type chains of gold nanoparticles encapsulated within dielectric amyloid protein nanofibrils of alpha-synuclein. *Angew. Chem. Int. Ed. Engl.* **2011,** *50* (6), 1332-7.

93. Zhou, W. B.; Freed, C. R., Tyrosine-to-cysteine modification of human alpha-synuclein enhances protein aggregation and cellular toxicity. *Journal of Biological Chemistry* **2004,** *279* (11), 10128-10135.

94. Lee, M. K.; Stirling, W.; Xu, Y. Q.; Xu, X. Y.; Qui, D.; Mandir, A. S.; Dawson, T. M.; Copeland, N. G.; Jenkins, N. A.; Price, D. L., Human alpha-

synuclein-harboring familial Parkinson's disease-linked Ala-53 -> Thr mutation causes neurodegenerative disease with alpha-synuclein aggregation in transgenic mice. *P Natl Acad Sci USA* **2002,** *99* (13), 8968-8973.

95. Tateishi, J.; Nagara, H.; Hikita, K.; Sato, Y., Amyloid Plaques in the Brains of Mice with Creutzfeldt-Jakob Disease. *Ann Neurol* **1984,** *15* (3), 278-280.

96. Hsiao, K.; Chapman, P.; Nilsen, S.; Eckman, C.; Harigaya, Y.; Younkin, S.; Yang, F. S.; Cole, G., Correlative memory deficits, A beta elevation, and amyloid plaques in transgenic mice. *Science* **1996,** *274* (5284), 99-102.

97. Dugger, B. N.; Serrano, G. E.; Sue, L. I.; Walker, D. G.; Adler, C. H.; Shill, H. A.; Sabbagh, M. N.; Caviness, J. N.; Hidalgo, J.; Saxon-LaBelle, M.; Chiarolanza, G.; Mariner, M.; Henry-Watson, J.; Beach, T. G.; Consortium, A. P. s. D., Presence of Striatal Amyloid Plaques in Parkinson's Disease Dementia Predicts Concomitant Alzheimer's Disease: Usefulness for Amyloid Imaging. *J Parkinson Dis* **2012,** *2* (1), 57-65.

98. Paik, S. R.; Lee, J. H.; Kim, D. H.; Chang, C. S.; Kim, J., Aluminum-induced structural alterations of the precursor of the non-A beta component of Alzheimer's disease amyloid. *Arch Biochem Biophys* **1997,** *344* (2), 325-334.

99. Lee, J. H.; Lee, I. H.; Choe, Y. J.; Kang, S.; Kim, H. Y.; Gai, W. P.; Hahn, J. S.; Paik, S. R., Real-time analysis of amyloid fibril formation of alpha-synuclein using a fibrillation-state-specific fluorescent probe of JC-1. *Biochem J* **2009,** *418* (2), 311-23.

100. Yang, C. H.; Wang, M. X.; Haider, H.; Yang, J. H.; Sun, J. Y.; Chen, Y. M.; Zhou, J. X.; Suo, Z. G., Strengthening Alginate/Polyacrylamide Hydrogels Using Various Multivalent Cations. *Acs Applied Materials & Interfaces* **2013,** *5* (21), 10418-10422.

101. Sun, J. Y.; Zhao, X. H.; Illeperuma, W. R. K.; Chaudhuri, O.; Oh, K. H.; Mooney, D. J.; Vlassak, J. J.; Suo, Z. G., Highly stretchable and tough hydrogels. *Nature* **2012,** *489* (7414), 133-136.

# 초록

## 알파-시누클레인의 대체자가결합을 이용한 2차원 단백질 필름과 3차원 단백질 마이크로스피어의 제작과 응용

단백질의 자가조립현상을 이해하고 조절하는 것은 병리학적 측면뿐만 아니라, 단백질 기반 재료들의 소재를 다양화 한다는 측면에서 중요성을 찾을 수 있다. 본 논문에서는, 자가 결합성 단백질인 알파-시누클레인 (α-Synuclein, αS)의 대체자가결합을 유도하여, 2차원 단백질 필름 구조체와 3차원 단백질 구형 구조체 (Protein microsphere)를 제작하였다. 알파-시누클레인의 단입자에 일반적인 배양 온도인 37 ℃ 대신, 50 ℃ 의 고온 처리를 통하여 2차원 단백질 필름 구조체를 제작하였다. 단백질 필름 구조체는 수백 나노미터의 너비로 제작되었으며, 40 nm의 높이로 형성됨을 원자현미경상에서 확인 하였다. 이러한 대체자가결합은, 알파-시누클레인의 뮤턴트인 Y136C와 시스테인에 결합하는 형광염료인 Alexa Flour 488간 결합체의 배양을 통해 역시 확인되었다. 필름구조물은 고해상도적외선분광계(FTIR) 상에서 단입자가 나타내는 임의구조의 형태가 줄어들고, 소폭의 베타-병풍구조가 발현되었지만, 그 베타-병풍 구조의 증가 정도는 아밀로이드 구조체와 대비하였을 때 소폭으로 평가되었다. 이 현상을 기반으로 알파-시누클레인의 필름화 현상이 물-공기 계면을 매개로 이루어지는 가설을 바탕으로, 물-기름 계면의 제공을 통해 동일 높이로 형성되는 단백질 필름의 크기를 마이크로미터 단위까지 확장하였다. 확장시킨 단백질 필름은 알파시누클레인과 상호작용하는 폴리머 중 하나인 10,12-Pentacosadiynoic acids (PCDA)와 반응시켜 55 nm의 높이를 갖는 PCDA-αS 하이브리드 필름 구조체를 제작하였다. 이 필름구조체는 자외선을 통해 PCDA의 파이결합이 유도되어 파란색으로 관찰되었고, 추가적인 열처리를 통해 빨간색으로 변화되었다. 이렇게 형성된 PCDA-αS 하이브리드 필름은 단백질로만 이루어진 필름구조체에 대비하여 물리적, 화학적으로 높은 안정성을 보였다. 추가적으로, 형성된 파란색상태의 PCDA-αS 필름은 유기용매, pH, 온도에 특이적으로 반응하여 색 변화를 나타내었고, 특히 열자극을 통해 빨강 상태로 변환되었을 때 높은 전기전도성이 관찰되었다. 알파-시누클레인 필름은 세포부착실험과 나노입자로 구성된 필름에 대한 흡착실험을 통해 생체친화적인 단백질 재료로써의

응용성이 확인되었다. 한편, 알파-시누클레인의 올리고머를 이용하여 기존에 나노섬유체가 아닌 단백질 구형구조체로의 대체자가결합이 유도되었다. 알파-시누클레인 구형구조체의 형성은 급속냉각으로 이루어지는 동시다발적인 얼음결정 형성으로부터 유도된 단백질의 부분적인 초고농도화와, 냉동 보관상태에서 유도되는 얼음결정 사이에 존재하는 단백질-물분자의 유사-액체층(Quasi liquid layer, QLL)에서 일어나는 알파-시누클레인 올리고머의 구조변형, 그리고 단백질의 초고농도화로부터 유도되는 단백질-물분자 액상구조(Glass state)의 동결건조에서 나타나는 커피-얼룩 효과(Coffee stain effect)로부터  기인한다. 형성된 단백질 구형구조체는 상온에서 안정적인 형태로 유지되었는데 이것은 부분적인 베타-병풍구조에서 기인한다. 이 구형구조체는 알파-시누클레인 올리고머와 형광염료인 에오신(Eosin)의 결합체로 제작한 구조체를 형광현미경으로 분석함으로써 중공형 구조임을 확인하였고, 주사전자현미경(Scanning electron microscope, SEM)의 집속이온빔(Focused ion beam, FIB)을 사용한 부분절단으로도 중공형 구조를 확인하였다. 단백질 구형구조체는 온도조절을 통해 추가적인 자가결합이 유도 될 수 있었으며, 형성된 구조물은 유사-밤송이 구조의 아밀로이드 구조로 형성되는 것을 전자현미경을 통해 확인하였다. 이러한 성질을 이용하여, 구조체를 하이드로젤에 도입하여 하이드로젤 내부에 나노스케일 네트워크를 추가적으로 도입함으로써 하이드로젤의 물성을 개선하였다. 제작된 알파-시누클레인 마이크로스피어로부터 유래되는 섬유화 단백질의 유사-밤송이 구조로의 구조변형은, 다양한 퇴행성질환 환자의 뇌세포 주변에서 관찰되는 마이크로 단위의 아밀로이드반(Amyloid plaque)의 형성을 설명하는데 도움을 줄 수 있다. 종합하면, 본 논문에서는 알파-시누클레인의 대체 자가결합을 유도하여 안정한 대체자가결합 물질들을 제안하였으며, 이를 기반으로 섬유화 단백질의 자가결합에 대한 이해를 높였다는점에서 의의를 갖는다. 나아가 섬유화 단백질 기반의 재료들을 제안하고 단백질 재료로써 활용될 수 있는 활용예에 대한 제시를 통해 섬유화 단백질을 소재로써 활용할 수 있는 범위를 확장시켰다는 측면에서 연구의 중요성을 찾을 수 있다.